EBioMedicine 65 (2021) 103250

Contents lists available at ScienceDirect

EBioMedicine

journal homepage: www.elsevier.com/locate/ebiom

Development of a novel, fully human, anti-PCSK9 antibody with potent hypolipidemic activity by utilizing phage display-based strategy

Menglong Xu[a], Gaoxin Lei[a,b], Manman Chen[a], Ke Wang[a], Wenxiu Lv[a], Panpan Zhang[a], Tuo Hu[a], Jie Gao[a], Chenchen Lu[a], Ying Mei[a], Zhipan Xu[a], Zhengli Bai[a], Huajing Hu[a], Yiwei Jiang[a], Shuhua Tan[a,*]

[a] Department of Cell and Molecular Biology, School of Life Science and Technology, State Key Laboratory of Natural Medicines, Jiangsu Key Laboratory of Druggability of Biopharmaceuticals, China Pharmaceutical University, Nanjing 210009, P.R. China
[b] Vaccine Engineering Center of China Medical City, Taizhou 225300, Jiangsu Province, P.R. China

ARTICLE INFO

Article History:
Received 17 November 2020
Revised 27 January 2021
Accepted 3 February 2021
Available online xxx

Keywords:
PCSK9
Phage display
Human antibody
Affinity maturation
Hypercholesterolemia

ABSTRACT

Background: Proprotein convertase subtilisin/kexin type 9 (PCSK9) regulates serum LDL cholesterol (LDL-C) levels by facilitating the degradation of the LDL receptor (LDLR) and is an attractive therapeutic target for hypercholesterolemia intervention. Herein, we generated a novel fully human antibody with favourable druggability by utilizing phage display-based strategy.

Methods: A potent single-chain variable fragment (scFv) named AP2M21 was obtained by screening a fully human scFv phage display library with hPCSK9, and performing two *in vitro* affinity maturation processes including CDR-targeted tailored mutagenesis and cross-cloning. Thereafter, it was transformed to a full-length Fc-silenced anti-PCSK9 antibody FAP2M21 by fusing to a modified human IgG1 Fc fragment with L234A/L235A/N297G mutations and C-terminal lysine deletion, thus eliminating its immune effector functions and mitigating mAb heterogeneity.

Findings: Our data showed that the generated full-length anti-PCSK9 antibody FAP2M21 binds to hPCSK9 with a K_D as low as 1.42 nM, and a dramatically slow dissociation rate (k_{off}, 4.68×10^{-6} s^{-1}), which could be attributed to its lower binding energy (-47.51 kcal/mol) than its parent counterpart FAP2 (-30.39 kcal/mol). We verified that FAP2M21 potently inhibited PCSK9-induced reduction of LDL-C uptake in HepG2 cells, with an EC_{50} of 43.56 nM. Further, in hPCSK9 overexpressed C57BL/6 mice, a single tail *i.v.* injection of FAP2M21 at 1, 3 and 10 mg/kg, dose-dependently up-regulated hepatic LDLR levels, and concomitantly reduced serum LDL-C by 3.3% (P = 0.658, unpaired Student's t-test), 30.2% (P = 0.002, Mann-Whitney U-test) and 37.2% (P = 0.002, Mann-Whitney U-test), respectively.

Interpretation: FAP2M21 with potent inhibitory effect on PCSK9 may serve as a promising therapeutic agent for treating hypercholesterolemia and associated cardiovascular diseases.

1. Introduction

Hypercholesterolemia, particularly an increase in circulating low-density lipoprotein cholesterol (LDL-C), predisposes to the development of cardiovascular diseases (CVDs) which constitute the leading cause of mortality globally [1]. LDL-C in circulation is primarily cleared by hepatocellular LDL receptor (LDLR)-mediated endocytosis. Once serum LDL particles bind to the cell surface LDLR of hepatocytes, internalization of the LDL/LDLR complexes is initiated through clathrin-dependent endocytosis, and then LDL-C is directed to lysosomes for degradation while LDLR recycles back to the plasma membrane [2].

Proprotein convertase subtilisin/kexin type 9 (PCSK9) is a secretory serine protease composed of 692 amino acids and principally

Abbreviations: ADCC, antibody-dependent cellular cytotoxicity; BLI, bio-layer interferometry; BSA, bovine serum albumin; CVD, cardiovascular disease; CDR, complementarity-determining region; CDC, complement-dependent cytotoxicity; CTD, C-terminal domain; EGF-A, epidermal growth factor-like repeat A; Fab, antibody-binding fragment; GAPDH, glyceraldehyde 3-phosphate dehydrogenase; HC, heavy chain; HDL-C, high-density lipoprotein cholesterol; HDD, hydrodynamic delivery; HNF1, hepatocyte nuclear factor 1; IMAC, immobilised metal affinity chromatography; LC, light chain; LDLR, low-density lipoprotein receptor; LDL-C, low-density lipoprotein cholesterol; mAbs, monoclonal antibodies; MMPBSA, molecular mechanics-poison boltzmann surface area; NS, nephrotic syndrome; PBS, phosphate-buffered saline; PCSK9, proprotein convertase subtilisin/kexin type 9; LPEI, linear polyethyleneimine; scFv, single-chain variable fragment; TC, total cholesterol; TG, triglyceride

* Corresponding author.
E-mail address: tanshuhua163@163.com (S. Tan).

https://doi.org/10.1016/j.ebiom.2021.103250

Research in Context section

Evidence before this study

Previously, multiple PCSK9 inhibitors have been shown to enhance hepatocyte clearance of plasma LDL-C by reducing the degradation of LDL-R and may serve as a useful supplement or replacement for statin therapy. Among PCSK9 inhibitors, two fully human mAbs against PCSK9 derived from transgenic mice platforms have entered clinic use as LDL-C-lowering drugs. Notably, other than transgenic mice, phage display technology is an alternative powerful platform to generate fully human mAbs. Thus, this study was designed to develop a highly potent human antibody against PCSK9 with favourable druggability by utilizing phage display-based strategy for future therapeutic applications.

Added value of this study

Herein, we describe the discovery, affinity maturation and characterization of a novel fully human mAb (FAP2M21) against PCSK9 from a naïve human phage library. Our data showed that the generated fully human, anti-PCSK9 IgG1 mAb FAP2M21 binds to PCSK9 with a K_D as low as 1.42 nM, and a dramatically slow dissociation rate (k_{off}, 4.68 $\times$ 10^{-6} s^{-1}). *In vitro* tests indicated that FAP2M21 significantly up-regulated LDLR levels and potently inhibited the PCSK9-induced reduction of LDL-C uptake in HepG2 cells, with an EC_{50} of 43.56 nM. *In vivo* functional studies demonstrated that FAP2M21 dramatically reduced the serum LDL-C and TC levels in hPCSK9 overexpressed C57BL/6 mice model after a single tail *i.v.* injection of FAP2M21 at doses of 1−10 mg/kg. The data demonstrate that FAP2M21 is a novel potent fully human anti-PCSK9 IgG1 mAb derived from human phage library, and the extremely slow dissociation rate it possesses appears to be favourable to its druggability.

Implications of all the available evidence

FAP2M21 is a novel potent fully human anti-PCSK9 IgG1 mAb discovered by utilizing phage display-based strategy. It binds to PCSK9 with a K_D as low as 1.42 nM, and a dramatically slow dissociation rate (k_{off}, 4.68 $\times$ 10^{-6} s^{-1}), and potently inhibits PCSK9-mediated LDLR degradation and robustly reduces the serum LDL-C and TC levels in a hyperlipidemic mouse model, suggesting that FAP2M21 possesses favourable druggability and may serve as a promising candidate for treating hypercholesterolemia and associated cardiovascular disease.

synthesized in hepatocytes [3]. As a well-known indirect regulator of serum LDL-C, the secreted PCSK9 in circulation binds to the epidermal growth factor-like repeat A (EGF-A) domain of the LDLR on the liver cell surface, and directs the LDLR towards lysosomal degradation rather than recycling to the cell surface, thereby decreasing the hepatic uptake of LDL-C [4−6]. Hence, inhibiting PCSK9 synthesis, secretion or blocking its interaction with LDLR can facilitate LDLR recycling, thereby enhancing LDL-C clearance and reducing the risk of CVDs [7]. Besides, PCSK9 has been found to be upregulated in hepatocytes in nephrotic syndrome (NS) and obese subjects, as well as statin-treated patients [8−10], which allows it to be an attractive therapeutic target for these metabolic disorder diseases. So far, two fully human anti-PCSK9 antibodies including evolocumab and alirocumab developed by transgenic mice platforms have been approved for treating hypercholesterolemia in clinic [11].

Notably, other than transgenic mice platforms, phage display technology, which was awarded the 2018 Nobel Prize in Chemistry, provides an alternative powerful platform to discover fully human mAbs [12]. In principle, human antibody proteins such as single-chain variable fragments (scFvs) or antigen-binding fragments (Fabs) are displayed on the surface of the filamentous phage, which allows the *in vitro* screening of human antibodies against almost any antigens even including toxins and non-immunogenic antigens [13]. Since the antibodies derived from a naïve library have not gone through an *in vivo* somatic hypermutation process, further *in vitro* affinity maturation is usually needed to achieve high-affinity antibodies [14]. For example, the first marketed fully human mAb (adalimumab) against tumour necrosis factor-α (TNF-α), which was approved by the US FDA for the treatment of moderate to severe rheumatoid arthritis in December 2002, was developed by using phage display technology [15]. To date, numerous phage display-derived antibodies have been approved or under advanced clinical investigation [13,16,17]. Phage display strategy has proven to be a valuable, robust, and efficient approach to discover and develop human therapeutic antibodies.

Herein, we explored to discover a highly potent human mAb against human PCSK9 (hPCSK9) by using phage display technology. First, a naïve phage-displayed human scFv library was screened by biopanning to identify a lead candidate with modest binding affinity to hPCSK9. Second, the parental scFv was subjected to *in vitro* affinity maturation via parallel CDR walking mutagenesis targeting the key amino acids in CDR loops using one-step mutagenesis PCR [14,18,19]. Third, cross-cloning was performed to achieve the exchange of CDR regions of several most improved variants which leave framework regions unperturbed [20,21], so as to generate a highly potent human scFv antibody against PCSK9. Thereafter, a full-length human anti-PCSK9 antibody FAP2M21, with a high affinity for hPCSK9 and a dramatically slow dissociation rate, as well as potent *in vivo* hypolipidemic activity, was developed.

2. Methods

2.1. Reagents and antibodies

MEM (Cat# 41500034), Opti-MEM (Cat# 31985070) and Pluronic-F68 (Cat# 9003-11-6) were purchased from Thermo Fisher Scientific (Waltham, MA, USA). Fetal bovine serum (Cat# F2442), penicillin G sodium salt (Cat# PENNA) and streptomycin solution (Cat# 5711) were obtained from MilliporeSigma (Burlington, MA, USA). The linear polyethyleneimine (Cat# 23966, LPEI, 25 KDa) was purchased from Polysciences (Warrington, Pennsylvania, USA). HyClone™ HyCell™ CHO Medium (Cat# SH30933.02) was purchased from GE Healthcare (Piscataway, NJ, USA). Bovine serum albumin (Cat# 9048−46-8) was obtained from Biofroxx (Einhausen, Hessen, Germany). Agarose Gel DNA Extraction Kit (Cat# 9762) and *Dpn* I (Cat# 1609) were bought from TaKaRa (Dalian, Liaoning, China). Rabbit anti-PCSK9 antibody (Cat# ab181142) and rabbit anti-LDLR antibody (Cat# ab52818, RRID:AB_881213) were obtained from Abcam (Cambridge, UK). HRP-conjugated mouse anti-M13 antibody was obtained from Sino Biological (RRID:AB_2857926, Cat# 11973-MM05T-H, Beijing, China). RIPA lysis buffer was obtained from Solarbio (Cat# R0020, Beijing, China). Phenylmethyl sulfonyl fluoride (PMSF) was purchased from Amresco (Cat# M145-5G, Solon, OH, USA). Glutamine (Cat# A600224), TMB substrate (Cat# A600954), IPTG (Cat# A100487), rabbit anti-GAPDH antibody (Cat# D110016), HRP-conjugated goat anti-rabbit IgG (Cat# D110058) and Alexa Fluor 488®-conjugated goat anti-rabbit IgG (Cat# D110061) were bought from BBI (Toronto, ON, Canada). LDL labelled with 1, 1'-dioctadecyl - 3, 3, 3', 3'-tetramethyl- indocarbocyanine perchlorate (DiI-LDL) was obtained from Yiyuan Biotechnologies (Cat#YB-0011, Guangzhou, Guangdong, China). Assay kits for LDL-C (Cat# A113-1), TC (Cat# A111-1), TG (Cat# A110-1) and HDL-C

(Cat# A112-1) were obtained from Nanjing Jiancheng Bioengineering Institute (Nanjing, Jiangsu, China).

2.2. Cell cultures

Human hepatic HepG2 cells (RRID:CVCL_0027) were obtained from China Infrastructure of Cell Line Resources (Beijing, China) and validated by short tandem repeat (STR) DNA fingerprinting. The cells were maintained at 37 °C,5% CO_2, in MEM supplemented with penicillin (100 U/mL), streptomycin (100 μg/mL) and 10% (v/v) fetal bovine serum (FBS). Chinese hamster ovary (CHO-3E7) cells (RRID: CVCL_JY74) were obtained from GenscriptBiotech (Nanjing, Jiangsu, China) and cultured in HyClone™ HyCell™ CHO Medium, supplemented with 4 mM glutamine and 0.1% (w/v) Pluronic-F68, in a humidified 37 °C incubator shaker under constant agitation rate (120 rpm) with 5% CO2.

2.3. Antigen preparation

The coding sequence of hPCSK9 (Genbank accession number: NM_174936.3) fused with a Kozak consensus sequence (GCCGCCACC) [22] at the 5'-end and a 6 × His-tag gene at the 3'-end was synthesized at Genscript Biotech and subcloned into the mammalian expression vector pTT5 at *Eco*R I/*Hin*d III restriction sites (Fig. S1). After confirmed by sequencing, the construct was transfected into CHO-3E7 cells by using 25 KDa LPEI for the transient expression of hPCSK9 protein [23]. After transfection for 7 days, the culture supernatant was harvested by centrifugation at 12000 × g for 20 min. Then, hPCSK9 was purified using Ni^{2+} Based immobilized metal ion affinity chromatography (Ni-IMAC, GE Healthcare), followed by Superdex™ 200 HR 10/300GL size-exclusion chromatography (GE Healthcare) according to the manufacturer's instructions. Protein concentration was quantified by using the BCA protein assay kit (Biomiga, San Diego, CA, USA).

2.4. Library panning

Four rounds of panning were performed in immune tubes (Nunc, Roskilde, Denmark) coated with recombinant hPCSK9 using a fully human naive scFv phage display library, which was previously constructed in our lab [24]. Briefly, the immune tubes were coated with two-fold serial dilution concentration of PCSK9 (60, 30, 15 and 7.5 μg/mL for each round) in carbonate buffer (pH 9.6) at 4 °C overnight. After blocked with 4 mL PBS containing 2% (w/v) skim milk, the antigen-coated tube was incubated with amplified phage particles at 25 °C for binding for 120 min (the time for the remaining three rounds was 100, 80 and 60 min, respectively). The unbound phages were removed by washing with 0.1% (v/v) Tween-20/PBS for five times (10, 15 and 20 times for later rounds), while the bound phages were eluted by 1 mL of 100 mM triethylamine (pH 12) and used to infect exponentially growing *E. coli* TG1 cells for next round of panning.

2.5. Monoclonal phage ELISA

Enriched clones obtained from the fourth round of panning were spread on 2 × YT-AG plates (2 × YT medium with 100 μg/mL Amp and 2% (w/v) Glucose) and randomly picked for monoclonal phage ELISA analysis as previously described [24]. Phage-scFv clones were considered as positive clones if the absorbance signals were three times greater than the absorbance obtained with BSA. M13KO7 helper phage was also served as a negative control in this assay. Besides, noncompetitive phage ELISA with the addition of increasing titers of phages (10^3, 10^4, 10^5, 10^6, 10^7, 10^8, 10^9, 10^{10} pfu/ml) and competitive phage ELISA with the addition of increasing amounts of free hPCSK9 (10, 10^2, 10^3, 10^4, 10^5, 10^6, 10^7 pg per well) were also set up to further compare the sensitivity and specificity of the most positive phage clones [25].

2.6. Construction of scFv Mutant Library

Construction of the parental PCSK9 binding scFv mutant library was performed parallelly for six complementary determination regions (CDRs) by PCR mutagenesis. In brief, the six CDR loops were determined using the AbM definition schemes issued by Oxford Molecular's AbM antibody modelling software [26,27]. Five of the CDR loops (HCDR1, HCDR2, LCDR1, LCDR2 and LCDR3) were submitted to canonical structure prediction and amino acid frequencies analysis in the abysis database (www.bioinf.org.uk) [28], and then the degenerate oligomers for these five CDR loops (Table 1) were designed based on the amino acid preferences as described previously [29,30]. For HCDR3, the degenerate oligonucleotides (Table 1) with the NNS codon (N randomizing with all four nucleotides and S introducing only C or G) were designed to introduce random mutations to the hotspots (RGYW and AGY) [14] since this hypervariable region is not applicable to the canonical clustering method. Afterwards, CDR-targeted semi-random mutagenesis was performed by one-step mutagenesis PCR [31] using the parental phagemid pCANTAB5-AP2 as a template. PCR products at 5.3 kb were gel-purified, digested with the restriction enzyme *Dpn* I (TaKaRa, Dalian, China) to remove the methylated template plasmid and transformed into TG1 electrocompetent cells. Library size was determined by serial dilution plating and colony counting.

2.7. Soluble expression and purification of scFv antibodies

The selected scFv genes were subcloned into the prokaryotic expression vector pET-27b (Novagen, Madison, WI, USA) at *Nco* I/*Hin*d III sites and transformed into *E. coli* BL21(DE3). Following induction with 0.2 mM IPTG at 16 °C for 20 h, the expressed soluble scFv with C-terminal 6 × His-tag was isolated from the periplasm and purified by a Ni-IMAC column (GE Healthcare), followed by size-exclusion chromatography on a Superdex™ 75.10/300 GL column (GE Healthcare) using PBS as the running buffer on a Biologic Duo Flow chromatography system (Bio-Rad, Hercules, CA, USA).

2.8. Real-time binding kinetics analysis

The binding kinetics of each antibody against hPCSK9 was analyzed by Bio-Layer Interferometry (BLI) using a ForteBio Octet QK^e System (ForteBio, Fremont, CA, USA) according to the manufacturer's instruction. All steps were performed at 30 °C with shaking at 1000 rpm. Briefly, hPCSK9 was biotinylated using a biotinylation kit (Genemore, Cat# G-MM-IGT, Shanghai, China) and immobilized on the surface of streptavidin biosensors for 300 s. Then, the hPCSK9-captured biosensors were dipped into two-fold series dilution of antibodies for 300 s or longer (association phase) and moved to assay buffer (PBS, pH 7.4, 0.02% Tween 20, 0.1% BSA) without analytes for 600 s (dissociation phase). The concentrations of scFv used were 3000, 1500, 750 and 375 nM, while the concentrations of mAb used were 800, 400, 200 and 100 nM, respectively. The kinetic constants including k_{on}, k_{off}, and K_D were analyzed by using ForteBio data analysis software ver. 7.1.

2.9. Western blot analysis

Western blot was performed to measure the protein expression levels in HepG2 cells or tissues as previously described [32]. The cells were washed with ice-cold PBS for three times and then lysed in cold RIPA lysis buffer (Solarbio, Beijing, China) containing 1 mM PMSF on ice for 30 min. Liver tissues were homogenized in ice-cold lysis buffer with 1 mM PMSF by using a glass homogenizer. After centrifugation

Table 1
Primers for the CDR-directed massive mutagenesis of AP2.

Primer	Sequence (5'-3')	Usage
AP2MUTH1-F	TGTGCAGCCTCTGGA**KDYNNSN**TC**NNSNNS**TAT**NNSNKSHV**CTGGGTCCGCCAGGCTCCAGGG	HCDR1
AP2MUTH1-R	CTGGCGGACCCA**GBDSMNSNN**ATA**SNNSNNG**AN**SNNRHM**TCCAGAGGCTGCACAGGAGAGTCT	HCDR1
AP2MUTH2-F	CTGGAGTGGGTCTCA**NNS**ATA**WVSNNSDVYDDYNNSNNSVNSNNS**TACGCAGACTCCGTGAAGGGC	HCDR2
AP2MUTH2-R	GGAGTCTGCGTA**SNNSNBSNNSNNRHHRBHSNNSBW**TAT**SNN**TGAGACCCACTCCAGCCCCTTCCC	HCDR2
AP2MUTL1-F	ATCTCTTGTTCTGGA**DVSNNST**CCAACATCGGA**NNSNNSNNS**GTA**WW**CTGGTACCAGCAGCTCCCAGG	LCDR1
AP2MUTL1-R	TGCTGGTACCAG**WW**TAC**SNNSNNSNN**TCCGATGTTGGA**SNNSBH**TCCAGAACAAGAGATGGTGACCCT	LCDR1
AP2MUTL2-F	AAACTCCTCATCTAT**NNSRHYNVYNNSCKBNNSW**CAGGGGTCCCTGACCGATTCT	LCDR2
AP2MUTL2-R	CAGGGACCCCTG**WSNNVMGSNNRBNRDYSNN**ATAGATGAGGAGTTTGGGAGCCGT	LCDR2
AP2MUTL3-F	GCTGATTATTACTGT**VVYDBY**TGGGATN**NS**AGCCT**GNNSNNSNNSK**TATTCGGCGGAGGGACCAAGC	LCDR3
AP2MUTL3-R	CTCCGCCGAATA**MSNNSNNSNN**CAGGCTSNNATCCCA**RVHRBBA**CAGTAATAATCAGCCTCATCCTC	LCDR3
AP2HOTH3-F	GTTGGTCAGGGGT**NSNNSNN**TTGGGGCCAAGGCACCCTGGTC	HCDR3
AP2HOTH3-R	GCCTTGGCCCCAA**NNSNNSN**ACCCCTGACCAACCGCCCTTCT	HCDR3
AP2HOTL3-F	CTGTGC**SNNS**TGGGATGAC**NNS**CTGTCGGCGCG**SNNS**TTCGGCGGAGGG	LCDR3
AP2HOTL3-R	GCCGAA**SNNS**CGCGCCGACAG**SNN**GTCATCCCA**SNNS**GCACAGTAATAA	LCDR3

The bold letters represent the mutated bases.

at 12,000 g for 15 min at 4 °C, the supernatant was harvested and total protein concentrations were determined using BCA protein assay kit (Biomiga, San Diego, CA, USA). An equal amount of protein from each sample was separated on 10% (w/v) SDS-PAGE and transferred onto a 0.22 μm polyvinylidene fluoride (PVDF) membrane (MerckMillipore, Darmstadt, Germany). The membrane was blocked with a solution of 0.1% (v/v) TBS-Tween 20 (TBST) containing 5% (w/v) nonfat milk at room temperature for 2 h, then incubated with corresponding primary antibodies against LDLR (Cat# ab52818, 1:1000), GAPDH (Cat# D110016, 1:1000) at 4 °C overnight, followed by incubation with appropriate horseradish peroxidase (HRP)-conjugated goat anti-rabbit IgG (Cat# D110058, 1:5000) at room temperature for 1 h. Protein bands were developed using ECL (Thermo Scientific, Massachusetts, USA) and quantified by ImageJ software (National Institutes of Health, Bethesda, MD, USA).

2.10. LDL-C uptake assay

The assay was performed as described previously [33] with slight modification. Briefly, HepG2 cells were maintained in MEM supplemented with 10% FBS. The cells were seeded in 96 well black plates at a density of 1×10^4 cells per well and grown to 70% confluence. Then, cells were pretreated with serum-free opti-MEM for 12 h, followed by treatment with 20 μg/ml PCSK9 protein alone or co-treatment with 50 μg/ml anti-PCSK9 scFv proteins for 8 h. Besides, for measuring EC_{50} values of the full-length antibodies, cells were treated with 50 nM hPCSK9 alone or in combination with increasing concentrations (1−500 nM) of anti-hPCSK9 mAbs. Thereafter, 15 μg/mL DiI-LDL was added, and the cells were incubated at 37 °C in the dark for an additional 4 h. Cells incubated with opti-MEM without Dil-LDL were used as negative control. Cells incubated with Opti-MEM and 15 μg/mL DiI-LDL were used as the control for normalization, respectively. After rinsing with PBS 3 times, LDL-C uptake was measured on a multimode microplate reader (Varioskan lux, Thermo scientific) at 520 nm excitation/580 nm emission.

2.11. Combination of improved CDRs from various scFv mutants (cross-cloning)

To further improve affinity, the independently improved CDRs from various scFv mutants were combined by the method of cross-cloning [20,21]. Primers (Table 2) were designed based on the framework region sequence from the parental AP2. Subsequently, overlap-extension PCR (OE-PCR) [34] was performed to amplify and assemble the cross-cloned gene fragments containing two or more optimized CDRs by using PrimeSTAR® HS DNA Polymerase (TaKaRa, Dalian, China). These amplified scFv fragments were digested with restriction enzyme *Nco* I and *Hin*d III (TaKaRa, Dalian, China), and cloned into the prokaryotic expression vector pET-27b (Novagen, Madison, WI, USA).

Table 2
Primers for the combination of improved CDRs.

Primer	Sequence (5'-3')
AP2H-FR1-F	CATGCCATGGATCAGGTCACCTTGAAGGAGTC
AP2L-FR4-R	CCCAAGCTTTTAGTGATGGTGGTGGTGATGACCTAGGACGGTCAGCTTGG
AP2H-FR2-F	GGTCCGCCAGGCTCCAGGGAAGG
AP2H-FR2-R	CCTTCCCTGGAGCCTGGCGGACC
AP2H-FR4-F	CCAAGGCACCCTGGTCACCGTCTCCTCA
AP2H-FR4-R	TGAGGAGACGGTGACCAGGGTGCCTTGG
AP2L-FR3-F	GGTCCCTGACCGATTCTCTGGCTCCAAG

2.12. Generation of full-length antibodies

To generate full-length antibodies, the heavy and light chain variable regions (VH and VL) of scFvs were fused with the constant region of modified human IgG1 heavy chain (HC) and human lambda light chain (LC, Genbank accession number: AAA59107.1) by gene synthesis at the Genscript Inc (Nanjing, China), respectively. The modified HC constant region contains triple Fc silencing mutations (L234A/L235A/N297G), known to eliminate antibody-dependent cell-mediated cytotoxicity (ADCC) and complement-dependent cytotoxicity (CDC) activity via abolishing the binding to Fcγ receptors (FcγRs) and complement protein C1q [35−38]. The C-terminal lysine residue in the heavy chain was also deleted to mitigate mAb heterogeneity caused by C-terminal lysine incomplete cleavage [39,40]. The synthesized full-length HC and LC genes containing a Kozak consensus sequence [22] followed by a signal peptide sequence at the 5'-end were subcloned into a mammalian expression vector pTT5 at *Eco*R I and *Hin*d III restriction sites, respectively. The signal peptides "MDWTWRFLFVVAAATGVQS" (Genbank accession number: CAA34971.1) and "MDMRVPAQLLGLLLLWLSGARC" (Genbank accession number: S24320) were used for the secretory expression of HC and LC, respectively. The resultant HC and LC expression plasmids (Fig. S2a and S2b) were co-transfected into suspension CHO-3E7 cells at 1:1 ratio (w:w) using LPEI for transient expression [23]. Seven days after transfection, the secreted IgGs in culture supernatant were purified by a protein A affinity chromatography (Roche, Mannheim, Germany).

2.13. Flow cytometry analysis

Flow cytometry analysis of the LDLR expressed on the cell surface was conducted as previously described [41], with slight modification. Following incubation with opti-MEM for 12 h, HepG2 cells were treated with 20 μg/ml hPCSK9 alone or co-treated with 20 μg/ml anti-PCSK9 mAbs for 12 h. Then, the cells were digested with trypsin,

detached by scraping and washed with PBS and collected in a 1.5 ml tube, then fixed in 200 μl of 4% (w/v) paraformaldehyde in PBS for 5 min at room temperature. Cells were incubated with 200 μl of 0.1% Tween in PBS (PBS-T) and blocked with 10% goat serum in 0.3 M glycine in PBS for 30 min, then incubated with rabbit anti-LDLR monoclonal antibody (Cat# ab52818, 1:100) for 30 min at room temperature, and followed by incubation with Alexa Fluor® 488-conjugated goat anti-rabbit IgG (Cat# D110061, 1:200) for 30 min at room temperature. After washing, the detection was performed directly on a Guava EasyCyte™ Flow Cytometry (Merck Millipore, Germany) at an excitation wavelength of 488 nm and an emission wavelength of 525 nm. The levels of LDLR on the cell surface were analyzed by using FlowJo software 7.6 (FlowJo, Oregon, USA) with 10,000 cells.

2.14. Immunofluorescence analysis

Detection of LDLR in HepG2 cells and liver tissues by immunofluorescence was performed as previously described [32,41] with minor modification. Briefly, after treatment, HepG2 cells were rinsed with PBS for 5 min for 3 times and fixed in 4% (w/v) para-formaldehyde in PBS for 30 min. Liver tissues were fixed in 4% (w/v) para-formaldehyde in PBS at 4 °C for 48 h, embedded in paraffin and sliced at 4 μm thickness. After deparaffinization and hydration, tissue sections were pretreated by heating for 20 min in sodium citrate solution (0.01 M, pH 6.0) in a 95 °C water bath for the antigen retrieval. Thereafter, the cells or tissue sections were blocked with 10% (v/v) goat serum in PBST for 1 h and incubated with rabbit anti-LDLR antibody (1:100, Cat# ab52818) overnight at 4 °C, followed by incubation with Alexa Fluor® 488-conjugated goat anti-rabbit IgG (1:200, Cat# D110061) for 1 h at room temperature and counterstained with DAPI (KeyGEN BioTECH, Nanjing, China) to show cell nucleus. Images were acquired by using Zeiss AX10 fluorescence microscopy (Zeiss, Oberkochen, Germany).

2.15. Homology modelling and molecular docking

The three-dimensional (3D) structure models of antibody Fv regions of FAP2M21 and FAP2 were built via homology modelling using the ABodyBuilder server (http://opig.stats.ox.ac.uk/webapps/abodybuilder) which could predict the 'canonical' CDR loops with sub-Angstrom accuracy [42]. Subsequently, the stereochemical quality of the constructed models was validated by Ramachandran plot in PROCHECK program (https://servicesn.mbi.ucla.edu/PROCHECK/). The constructed models were refined and docked with a high resolution 1.98 Å crystal structure of PCSK9 (PDB ID:2P4E) using the HDOCK web server (http://hdock.phys.hust.edu.cn/) [43], and the binding free energy (ΔG_{bind}) of the ten top-ranked binding poses were calculated using the Molecular Mechanics/GB Surface Area (MM/GBSA) method implemented in HawkDock web server (http://cadd.zju.edu.cn/hawkdock/) [44]. Then, the docked poses with the lowest binding free energies were selected as the best conformations, and the key interacting residues in those docked complexes were analyzed and mapped by the Pymol software Version 2.3.0 (Schrödinger, New York, USA).

2.16. Studies in mice

Six-week-old male C57BL/6 mice were obtained from Qinglongshan Experimental Animal Breeding Farm (SCXK (Su) 2017-0001; Nanjing, China) and maintained on a 12 h light/dark cycle at 25 °C. After acclimation for one week, mice were randomly divided into 8 groups (a normal group, a model group and six treatment groups, n = 6) using a computer random number generator. The hyperlipidemic mouse model was established by overexpressing hPCSK9 through hydrodynamic delivery (HDD) of 50 μg naked plasmid DNA (pTT5-hPCSK9) in 2 ml normal saline within 5 s [45, 46], while mice in normal control group were injected with empty vector/saline mixture. On the 6th day after HDD, elevated levels of serum hPCSK9 and lipid profiles in model mice were verified by ELISA and biochemical assays (data not shown). Then, mice in treatment groups were administrated a single *i.v.* injection of FAP2M21 and alirocumab at a dose of 1, 3, and 10 mg/kg, respectively. Mice in normal control group and model group were injected with saline (vehicle). At the end of the administration period, all mice were fasted for 8 h before blood sample collection, and then euthanized for tissue harvest. Liver tissues were dissected and separated into two parts, one was homogenized by RIPA buffer for protein isolation and subject to western blot assay, the other was fixed in 4% (w/v) paraformaldehyde and embedded in paraffin for histological examination.

2.17. Ethics

The experimental procedures for the *in vivo* studies were approved by the Animal Ethics Committees of China Pharmaceutical University (No. 201601179, 19 October 2016) and conformed to the Guide for the Care and Use of Laboratory Animals published by the National Institutes of Health.

2.18. Statistical analysis

All values were presented as means ± SEM and analyzed with GraphPad Prism 8.3.0 software (GraphPad Software, La Jolla, CA, USA). Normality of data was determined by the Kolmogorov–Smirnov normality test. Normally distributed variables between 2 independent groups were compared with unpaired Student t-test whereas non-normally distributed variables were analyzed with the Mann–Whitney U-test. A two-tailed value of $P < 0.05$ was considered statistically significant.

2.19. Role of funding source

The funding sources played no role in the study design, data collection, data analysis, interpretation, writing of the report, and the decision of paper submission.

3. Results

3.1. Selection of anti-PCSK9 scFv candidates from human scFv phage library

To isolate scFv candidates against PCSK9, the recombinant hPCSK9 (rhPCSK9) as the antigen was transiently expressed in CHO-3E7 cells, and purified by Ni^{2+} affinity chromatography and Superdex™ 200 size-exclusion chromatography. It was shown that the purified hPCSK9 has an expected molecular weight of about 62 KDa, and a purity of ≥ 95% as determined by 10% (w/v) SDS-PAGE under reducing condition (Fig. 1a and Fig. 1b).

A human scFv phage-displayed library constructed based on phagemid pCANTAB 5E vector (Fig. 1c) [24], was used for four rounds of panning. It was observed that the PCSK9-binding clones were clearly enriched (Fig. 1d). Further, over 2000 enriched clones were screened out by phage ELISA by using PCSK9-coated microplates, and 160 of them were considered as positive clones since their OD_{450} signals were at least 3-fold higher than the negative control. After sequencing these 160 strong binders, 15 unique scFvs originated from different germline genes (Table. S1) and containing at least one amino acid difference were identified and designated as AP1 to AP15.

By using monoclonal phage ELISA, it was verified that these 15 positive phage clones specifically react with hPCSK9 protein, but not to BSA (Fig. 1e). The affinities of the four most potent binders (AP2, AP4, AP5, and AP11) were further reconfirmed and compared based on the binding curve of noncompetitive phage ELISA and competitive phage ELISA. The

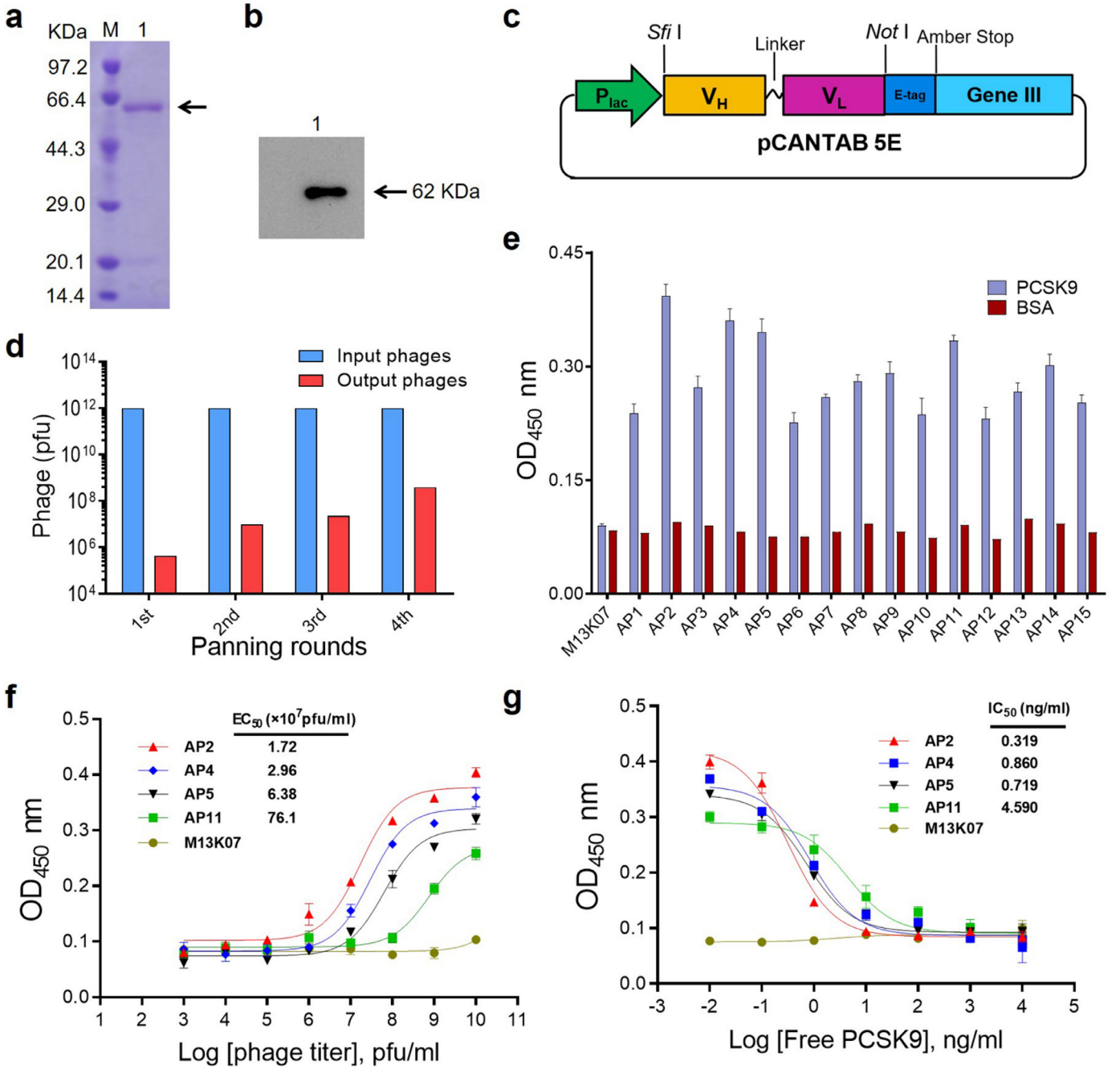

Fig. 1. Selection of anti-PCSK9 scFv antibodies by phage display. (a-b) Purified hPCSK9 was identified by 10% (w/v) SDS-PAGE (a) and western blot (b), M, molecular weight marker; Lane 1, purified hPCSK9 protein. (c) Scheme of phagemid vector pCANTAB 5E used for scFv display. (d) Enrichment of phage-displayed scFvs after each round of panning. In each panning round, the number of input phages was kept constant at 1×10^{12} pfu, and the output phages showed an enrichment by panning. (e) Screening of positive clones by monoclonal phage ELISA. Each phage-displayed scFv was tested against 5 μg/mL hPCSK9 or 5 μg/mL irrelevant BSA. (f-g) Characterization of four most potent binders by noncompetitive ELISA (f) and competitive ELISA (g). Serially 10-fold diluted phages alone or phages (1×10^{10} pfu/ml) mixed with serially 10-fold diluted free hPCSK9 were incubated in the wells immobilized with hPCSK9 (5 μg/mL). M13KO7 did not show any significant affinity to PCSK9 even at the concentration of 1×10^{10} pfu/mL and the highest affinity binder (AP2) was selected and used for further studies. Data are means ± SEM of 3 independent experiments.

data indicated that AP2 binds to hPCSK9 with the highest sensitivity (Fig. 1f), and this binding can be competitively inhibited by hPCSK9 in a concentration-dependent manner (Fig. 1g), demonstrating that AP2 is the strongest hPCSK9-specific wildtype binder.

3.2. Construction of scFv AP2 mutant library and selection of improved variants

To enhance the affinity for hPCSK9, parental scFv AP2 was subjected to *in vitro* affinity maturation by construction of AP2 mutant library and selection of improved variants. The library was constructed by CDR-directed massive mutagenesis using one-step mutagenesis PCR, and the degenerate oligomers were designed based on the CDR amino acid preferences (Fig. 2a) and hot-spot motifs (RGYW and AGY). An AP2 mutant library containing 4.2×10^7 independent transformants was thus established. Sequencing analysis of 30 randomly picked clones revealed that more than 93% of the transformants were mutated (data not shown). Then, AP2 mutants (named AP2M) with higher affinity for PCSK9 were enriched and selected by solid-phase sorting and phage ELISA as described above. As a result,

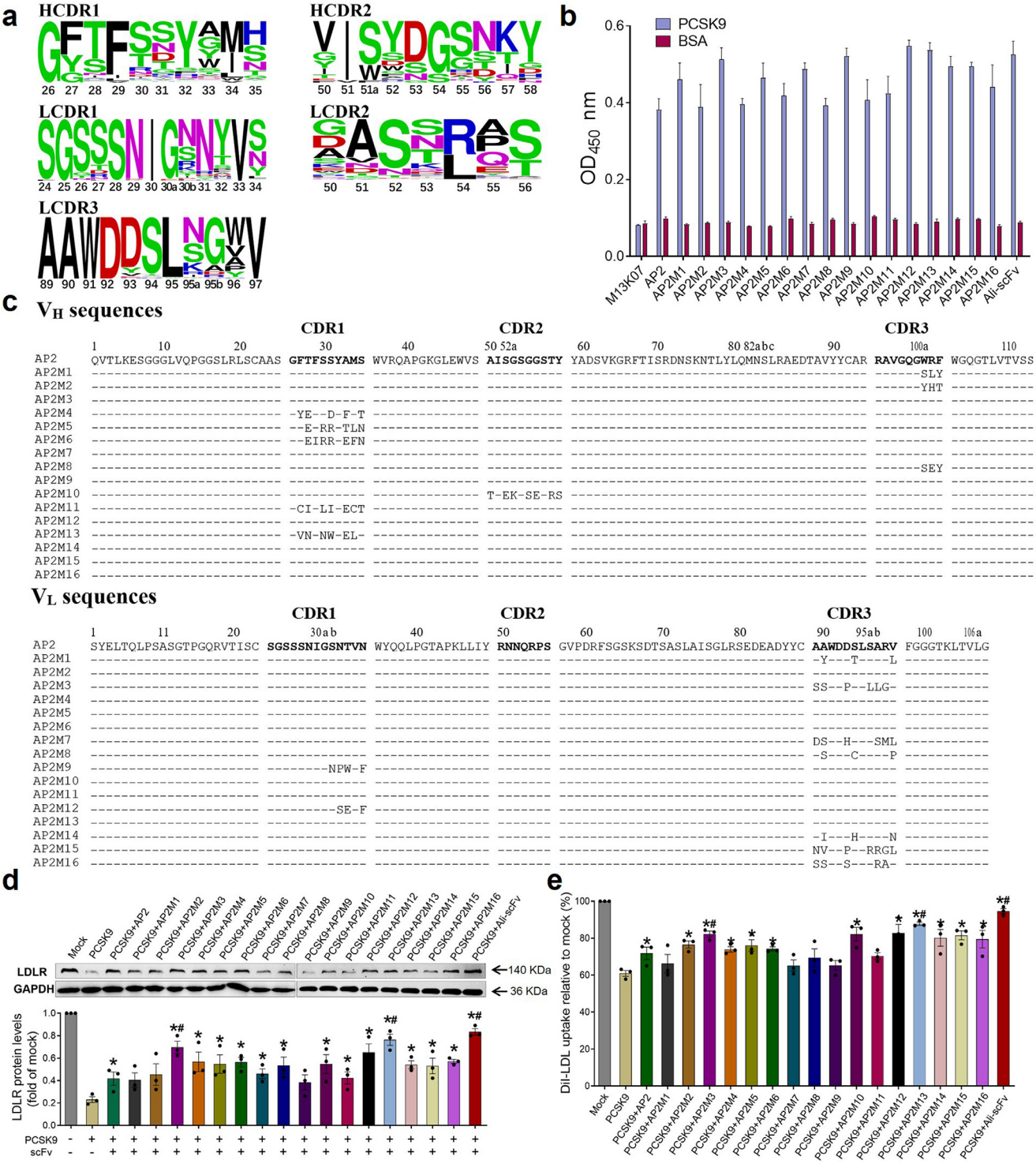

Fig. 2. Isolation of improved variants from AP2 Mutant Library. (a) The CDRs amino acid preferences of AP2 were depicted by using the sequence Logo tool (http://weblogo.berkeley.edu/logo.cgi). Symbol height corresponds to the relative frequency of each amino acid at each position. (b) Selection of AP2M with higher affinity to PCSK9 by monoclonal phage ELISA. (c) Sequence alignment of the V_H and V_L domains of AP2 with its corresponding variants (AP2M) isolated from the mutant library. Sequence numbering and CDR assignments (shown in bold letters) were done by using the abysis database at the URL of www.bioinf.org.uk/abs/. Dashes (-) represent the same residue as wild-type AP2. (d-e) Inhibitory effect of AP2 and AP2M on PCSK9-mediated LDLR degradation and LDL-C uptake reduction. HepG2 cells were treated with 20 μg/mL hPCSK9 with or without 50 μg/mL scFvs for 12 h, then LDLR protein levels were determined by western blot (d), DiI-LDL uptake levels were measured using a Multimode Reader (e), again normalized to that of the Mock group (vehicle control) for easier comparison. * $P< 0.05$ *vs.* PCSK9 treatment group. # $P< 0.05$ *vs.* AP2 treatment group (unpaired Student's t-test). Data are means ± SEM of 3 independent experiments.

16 unique mutants (Fig. 2c) displaying higher ELISA signals than parental AP2 (Fig. 2b) were identified.

The kinetic parameters of recombinantly expressed and purified AP2 and AP2 mutants (Fig.S3) binding to PCSK9 were further determined by BLI using a ForteBio Octet QK^e System. It was observed that 11 variants (AP2M1, AP2M3, AP2M5, AP2M6, AP2M8, AP2M9, AP2M10, AP2M12, AP2M13, AP2M14, AP2M15) showed 1.52 to 5.04-fold increase in affinity for PCSK9 as compared to the parental scFv

Table 3
Kinetic parameters of cross-cloned variants binding to hPCSK9.

Antibody	Origin	k_{on}($\times 10^3$ $M^{-1}s^{-1}$)	k_{off}($\times 10^{-3}$ s^{-1})	K_D(nM)	Fold increase
AP2	Parent	85.3 ± 11.7	7.44 ± 0.21	87.2 ± 12.2	1
AP2M3	HCDR3-optimization	45.9 ± 7.42	2.23 ± 0.10	48.7 ± 8.19	1.79
AP2M10	HCDR2-optimization	127 ± 18.7	3.32 ± 0.10	26.2 ± 3.92	3.33
AP2M12	LCDR1-optimization	91.4 ± 5.89	2.28 ± 0.05	25.0 ± 1.69	3.49
AP2M13	HCDR1-optimization	46.7 ± 3.32	0.83 ± 0.03	17.8 ± 1.43	4.90
AP2M14	LCDR3-optimization	57.2 ± 3.78	2.80 ± 0.06	48.9 ± 3.39	1.78
AP2M15	LCDR3-optimization	11.9 ± 1.07	0.68 ± 0.04	57.2 ± 6.34	1.52
AP2M17	Cross-cloning: 13 × 12	78.5 ± 8.44	1.14 ± 0.03	14.6 ± 1.63	5.97
AP2M18	Cross-cloning: 13 × 15	10.8 ± 0.10	0.54 ± 0.05	50.3 ± 6.44	1.73
AP2M19	Cross-cloning: 13 × 3	898 ± 721	10.7 ± 0.44	11.8 ± 0.96	7.39
AP2M20	Cross-cloning: 13 × 14	53.1 ± 5.25	1.51 ± 0.04	28.4 ± 2.90	3.07
AP2M21	Cross-cloning: 13 × 10	129 ± 14.5	0.47± 0.02	3.61 ± 0.44	24.2
AP2M22	Cross-cloning: 13 × 12 × 3	45.4 ± 5.43	0.61 ± 0.04	13.5 ± 1.88	6.46
AP2M23	Cross-cloning: 13 × 10 × 3	95.8 ± 18.4	4.15 ± 0.15	43.3 ± 8.45	2.01
AP2M24	Cross-cloning: 13 × 10 × 12	185 ± 73.4	1.91 ± 0.08	10.3 ± 4.13	8.47
AP2M25	Cross-cloning: 13 × 10 × 12 × 3	41.7 ± 6.72	1.85 ± 0.08	44.3 ± 7.39	1.97

(×) represents cross-cloned with. The rate constants were measured by BLI, $K_D = k_{off}/k_{on}$. Fold increase indicates the relative K_D improvement of variants *versus* the wild-type AP2. Errors are the standard error of the curve fit.

AP2 (K_D = 8.72 × 10^{-8} M), and displayed slower dissociation kinetics (k_{off}) than AP2 (Table. S2), which was basically consistent with the relative affinity observed in phage ELISA.

Additionally, we tested the effects of AP2 and AP2 mutants on the expression levels of LDLR and LDL-C uptake in HepG2 cells. As shown in Fig. 2d and e, six CDR-mutated variants (AP2M3, AP2M10, AP2M12, AP2M13, AP2M14 and AP2M15) most potently elevated the levels of LDLR and enhanced the LDL-C uptake in HepG2 cells as compared to the parental scFv AP2. Accordingly, we selected these six variants as lead candidates for further in vitro affinity maturation by using the cross-cloning method. Notably, although AP2M1 exhibited the highest affinity (K_D = 1.73 × 10^{-8} M) to hPCSK9, and displayed a markedly (4.1-fold) faster association rate (k_{on}, 3.52 × 10^5 M^{-1} s^{-1}), as well as a slightly (1.2-fold) slower dissociation rate (k_{off}, 6.08 × 10^{-3} s^{-1}) than AP2 (k_{on}, 8.53 × 10^4 M^{-1} s^{-1}, k_{off}, 7.44 × 10^{-3} s^{-1}), it did not show more potent hPCSK9 inhibitory effect as compared to the parental AP2, implying that higher binding affinity (K_D) dominated chiefly by faster association (k_{off}) might not result in stronger biological activity.

3.3. Cross-cloning of the improved variants

The selected AP2 variants were further cross-cloned to determine whether these combinations of improved CDRs from various scFv mutants could result in an increase in affinity and bioactivity. Thus, we cross-cloned AP2M13, the most potent HCDR1 optimized AP2 selected from the scFv AP2 mutant library, with AP2M3, AP2M10, AP2M12, AP2M14 and AP2M15 in different modes (see Table 3). The resultant clones (Fig. S4), named APM17-25, demonstrated a 1.7-24.2-fold increase in affinity as compared to the initial parental AP2, and 5/9 of these clones yielded an additional increase (1.2−4.9-fold) in affinity even compared with AP2M13. Of them, AP2M21 containing the optimized HCDR1 from AP2M13 and HCDR2 from AP2M10 showed the highest affinity (K_D = 3.61 nM) and the slowest off-rate (Table 3, Fig. 3a), and gained a 24.2-fold increase in affinity compared to the initial parental AP2.

We further evaluated the effects of the cross-cloned variants on the expression level of LDLR and LDL-C uptake in HepG2 cells. It was observed that AP2M21 exhibited the most potent activity in inhibiting the PCSK9-mediated degradation of LDLR and enhancing the LDL-C uptake in HepG2 cells (Fig. 3b, c). Interestingly, although AP2M18 (K_D=50.3 nM) had a much lower affinity for PCSK9 compared to AP2M21 (K_D=3.61 nM), the activity it showed was much close to AP2M21. The reason could be due to its markedly slow dissociation rate (off-rate) (Table 3), indicating that slow off-rate is a key element to increase the blocking effect of the antibody. Thus, we chose both AP2M21 and AP2M18 for further construction of the full-length antibodies and *in vivo* functional studies.

3.4. Generation and characterization of the full-length antibodies

Based on the parent scFv AP2, and the cross-cloned scFv variants AP2M21 and AP2M18, three full-length antibodies were constructed by fusing the V_H and V_L with a modified human IgG1 heavy chain constant region (C_H) with L234A/L235A/N297G mutations and C-terminal lysine deletion, and lambda light chain constant region (C_L), respectively. The resultant plasmids for HC and LC were co-transfected into CHO-3E7 cells for transient expression. After purification by a protein A affinity column, the full-length monoclonal antibodies were identified by 10% (w/v) non-reducing, and 12% (w/v) reducing SDS-PAGE gels, respectively (Fig. 4a). The data indicated that the purified full-length mAbs (FAP2M18, FAP2M21, FAP2 and alirocumab) consist of a 51 KDa heavy chain and a 23 KDa light chain.

We tested the activities of anti-PCSK9 mAbs to block PCSK9-mediated LDLR degradation by HepG2 cell-based assays. It was shown that hPCSK9 (20 μg/mL) dramatically induced LDLR degradation and resulted in a significant decrease of LDLR at the cell surface, whereas this reduction was effectively restored to different degrees in the presence of 20 μg/ml anti-PCSK9 mAbs (Fig. 4b-d).

Further, we verified whether anti-PCSK9 mAbs could enhance the function of LDL-C uptake in HepG2 cells. After treatment with hPCSK9 (50 nM) alone or with increasing concentrations (1−500 nM) of anti-PCSK9 mAbs, it was observed that these mAbs dose-dependently increased the LDL-C uptake by inhibiting PCSK9-mediated LDLR degradation in HepG2 cells. Among them, the full-length mAb FAP2M21 exhibited the most potent activity of increasing LDL-C uptake in HepG2 cells (EC_{50} = 43.56 nM), which was comparable to the positive control alirocumab (EC_{50} = 38.97 nM) (Fig. 4e).

3.5. Comparison of PCSK9-binding properties of FAP2M21 and its parental counterpart FAP2

To explain the strong neutralization potency of FAP2M21, we further explored the PCSK9-binding details of FAP2M21 and its parental FAP2. The BLI-based assay was firstly performed to visually compare the binding kinetics of these two mAbs in real-time. As shown in Fig. 5a, b and Table. S3, although both FAP2 and FAP2M21 bound to PCSK9 in a dose-dependent pattern, their binding modes were largely different. The parental antibody FAP2 exhibited a fast association rate (k_{on}, 1.76 × 10^5 M^{-1} s^{-1}) and fast dissociation rate (k_{off}, 5.76 × 10^{-2} s^{-1}) to PCSK9, while FAP2M21 displayed a moderate slower association rate (k_{on}, 3.33 × 10^3 M^{-1} s^{-1}) and a dramatically

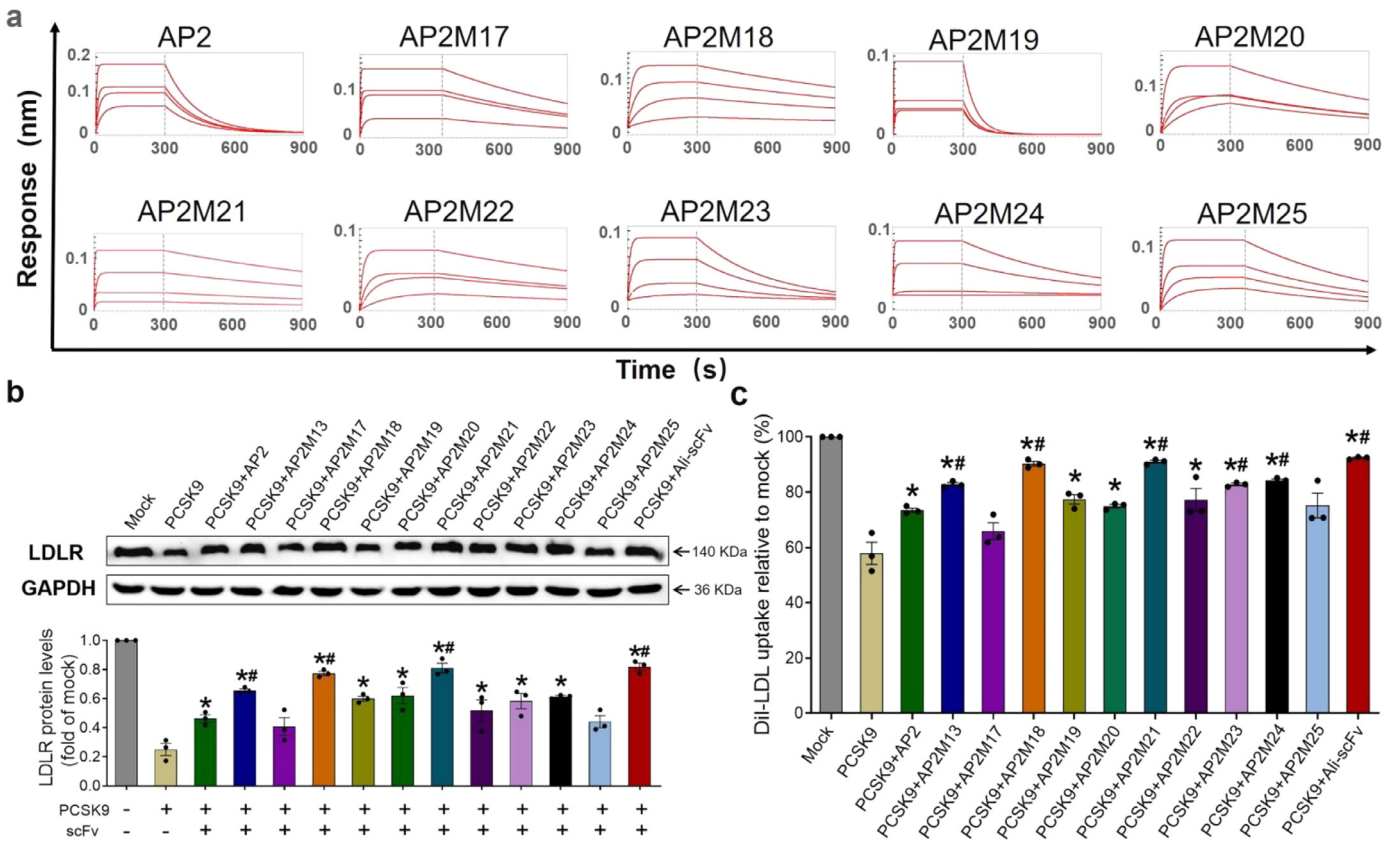

Fig. 3. Comparison and characterization of the cross-cloned variants. (a) BLI sensorgrams of cross-cloned AP2M as well as its parental AP2 (3000, 1500, 750, 375 nM) binding to biotin-labelled hPCSK9 immobilized on SA chip. Representative data for association/dissociation phases of each individual graphs were derived from the 1:1 fitting model (red lines). (b, c) Cross-cloned AP2M inhibit PCSK9-mediated LDLR degradation (b) and restore LDL-C uptake (c) in HepG2 cells. The LDLR protein levels and DiI-LDL uptake levels were measured and normalized as described above. * $P < 0.05$ *vs.* PCSK9 treatment group. # $P < 0.05$ *vs.* AP2 treatment group (unpaired Student's t-test). Data are means ± SEM of 3 independent experiments.

slower dissociation rate (k_{off}, 4.68 × 10^{-6} s^{-1}), thus yielding a ~23.3-fold higher affinity (K_D, 1.41 ± 0.13 nM *vs.* 32.8 ± 4.96 nM) as compared to FAP2. This data explained that the superior PCSK9 neutralization efficacy of FAP2M21 could be attributed to its extremely slow dissociation, which maximized and prolonged the duration of its inhibitory effect.

Additionally, the epitope−paratope interaction details for the high affinity of FAP2M21 to PCSK9 were detected by computer-based homology modelling. As shown in Fig. S5a and 5b, the three-dimensional (3D) structures of Fv regions of FAP2 and FAP2M21were built based on the highest identity template crystal structure (PDB code: 6APC, 93% and 86%identity in framework regions (FRs) of HC and LC, respectively). Subsequently, the CDR loops were predicted based on the canonical loop conformations. Model validation results revealed that more than 98.9 % of the residues were located in the most favoured regions and allowed regions of the Ramachandran plot (Fig. S5c, d), indicating these two modelled stereochemical structures are suitable for molecular docking analysis. The lowest binding energy (ΔG_{bind}) calculated by prime MM-GBSA was -30.39 kcal/mol for AP2-PCSK9, and -47.51 kcal/mol for AP2M21-PCSK9 (Table. S4), indicating that FAP2M21 appears to be more favourable for binding to PCSK9. By comparative analysis on these two complexes (Fig. 5c, d), it was found that the interaction residues of FAP2 including Ala24 in HFR1, Ser31 in HCDR2 and Arg94 in HCDR3 forms four hydrogen bonds against Asp212 and Gln256 in PCSK9 (Fig. 5c), while for FAP2M21, up to 12 residues are involved in the interaction, the exposed functional residues including Ser31 in HCDR1, Gly52A, Gly55 and Ser53 in HCDR2, Asp93 and Ser95A in LCDR3, form ten hydrogen bonds against Val536, Thr538, Ala542, Arg549, His551 and Arg592 in PCSK9 (Fig. 5d), respectively.

3.6. Hypolipidemic effect of FAP2M21 in mice over-expressing hPCSK9

To evaluate the lipid-lowering effect of FAP2M21 *in vivo*, hPCSK9 overexpressed hypercholesterolemic mice were generated by HDD injection of recombinant plasmid carrying hPCSK9 DNA sequence. On day 6 after HDD, the model mice exhibited a circulating hPCSK9 level of 1.15 μg/mL, and a 2.50-fold increase in serum LDL-C, 1.44-fold increase in serum TC and 1.47-fold increase in serum TG. Then, the mice in the treatment groups were given a single tail *i.v.* injection of FAP2M21 with various doses. After 18 h, a dose-dependent lowering of serum cholesterol was observed (Table 4). More specifically, treatment with FAP2M21 at 1, 3 and 10 mg/kg resulted in a 3.3% (P = 0.658, unpaired Student's t-test), 30.2% (P = 0.002, Mann-Whitney U-test) and 37.2% (P = 0.002, Mann-Whitney U-test) decrease in serum LDL-C relative to the model group, respectively (Fig. 6a). Also, it was verified that the levels of LDLR in liver tissues were dose-dependently up-regulated as assessed by immunoblotting (Fig. 6b) and immunostaining (Fig. 6c). In addition, FAP2M21 treatment significantly lowered the levels of serum TC and TG, but did not significantly affect serum HDL-C levels (Table 4).

4. Discussion

The aberrantly elevated level of serum low-density lipoprotein cholesterol (LDL-C) is a risk factor for cardiovascular disease [47,48]. Thus, reduction of LDL-C appears to be the major approach for the prophylaxis and treatment of CVD, and which could be achieved by both inhibiting LDL-C synthesis and accelerating LDL-C clearance. Statins, a class of specific hydroxy-3-methyl-glutaryl-CoA (HMG-CoA) reductase inhibitors, have been recommended as the first-line

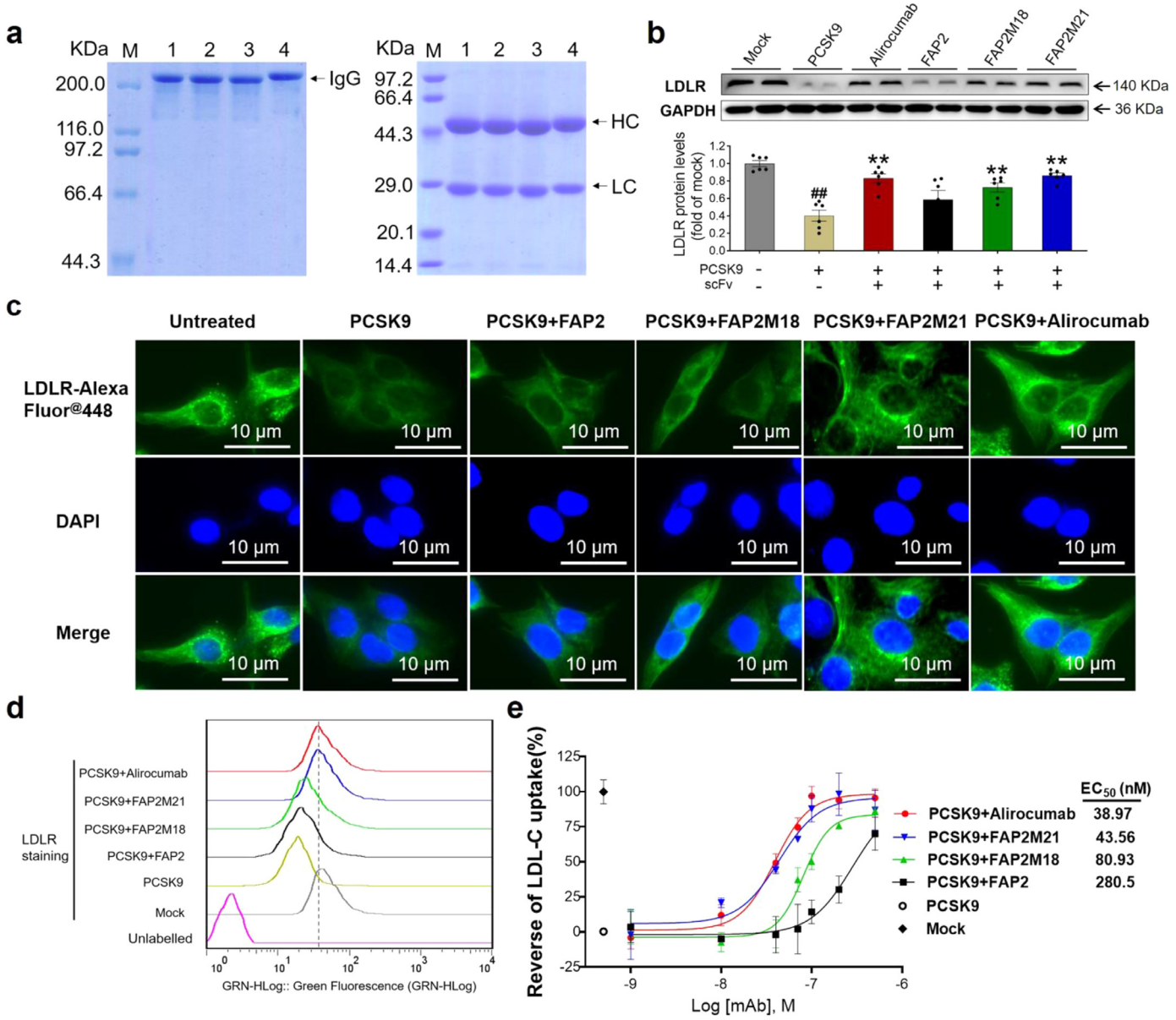

Fig. 4. Preparation and identification of anti-PCSK9 antibodies. (a) SDS-PAGE analysis of purified anti-PCSK9 mAbs under non-reducing (left panel, 10% gel) and reducing (right panel, 12% gel) conditions. M, molecular weight marker; Lane 1, FAP2; Lane 2, FAP2M18; Lane 3, FAP2M21; Lane 4, alirocumab. HC, heavy chain; LC, light chain. (b-d) HepG2 cells were treated with 20 μg/mL hPCSK9 alone or co-treated with 20 μg/mL anti-PCSK9 mAbs (FAP2, FAP2M18, FAP2M21, alirocumab) for 12 h, then the total LDLR protein levels in HepG2 were quantified by western blot analysis (b), and the cell surface LDLR protein levels were visualized by Immunofluorescence (c) and determined by flow cytometry (d) with excitation at 488 and emission at 525 nm. Scale bars, 10 μm. $^{**}P< 0.01$ *vs.* PCSK9 treatment group (Mann-Whitney U-test). $^{\#\#}P< 0.01$ *vs.* Mock group. (e) Effect of mAbs on PCSK9-mediated inhibition of LDL-C uptake in HepG2 cells. Dil-LDL uptake was measured in HepG2 cells incubated with 50 nM hPCSK9 alone or in combination with increasing concentrations (1−500 nM) of anti-PCSK9 mAbs. Quantification of fluorescence strength demonstrated that uptake of Dil-LDL by these mAbs was all dose-dependent. Data are given as means ± SEM (n = 3).

therapeutic drugs for lowering LDL-C in the management of patients with atherosclerotic cardiovascular disease risk by the American College of Cardiology (ACC)/American Heart Association (AHA) [49]. However, many high-risk CVD patients fail to achieve adequate LDL-C lowering efficacy on maximally tolerated statin doses [50]. In addition, some patients are statin-intolerant due to adverse effects, such as myopathy and increased activity of liver enzymes [2]. Accordingly, combination therapy of statins with other drugs would be a good choice in treating patients with a less than anticipated LDL-C lowering response and those unable to tolerate the recommended statin intensity.

Intriguingly, although statins have been previously unravelled to suppress the synthesis of endogenous cholesterol by competitively inhibiting HMG-CoA reductase and accelerate the clearance of circulation LDL-C through up-regulating hepatic LDLR [51–53], they concomitantly increase PCSK9 through inducing the expression of hepatocyte nuclear factor 1α (HNF-1α), the dominating transcription factor of PCSK9, thereby attenuating the LDL-C lowering effect of statins [54,55]. Thus, administration of statins in combination with PCSK9 inhibitor drugs would be a good solution to improve the LDL-C lowering efficacy of statins and address the issues of statin resistance and intolerance.

So far, multiple antibodies have been developed to lower serum LDL-C by selectively binding to PCSK9 to inhibit its interaction with the LDL-R, thereby keeping the normal recycling of LDL-R on the surface of hepatocytes. Of these antibodies, alirocumab and evolocumab, two fully human anti-PCSK9 antibodies derived from transgenic mice, have been approved by FDA and EMA and are currently used in

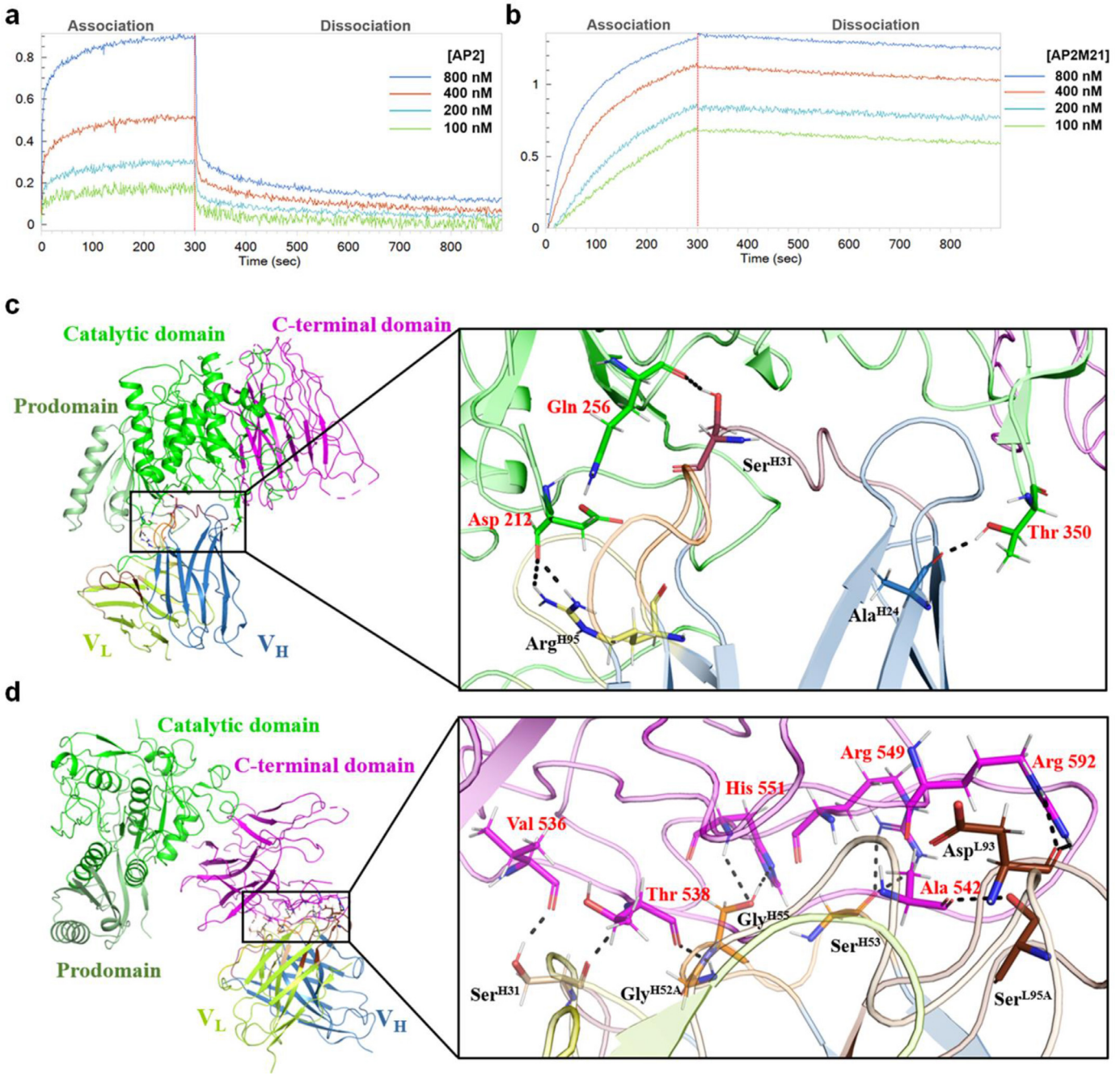

Fig. 5. Binding and interaction analysis of the mAbs to PCSK9. (a-b) Kinetics measurement of FAP2 (a) and FAP2M21(b) binding to surface-immobilized antigen hPCSK9 using a ForteBio Octet QK^e system. The biotinylated-hPCSK9 was loaded onto SA sensors and exposed to two-fold serial dilutions of antibody (800, 400, 200 and 100 nM) solutions for 300 s (association phase) followed by a dissociation phase of 600 s. Each concentration of analytes was shown in a different colour. (c-d) Intermolecular interaction analyses of the FAP2 (c) and FAP2M21 (d) with PCSK9. The prodomain, Catalytic domain and C-terminal domain of PCSK9 were coloured in palegreen, green and magenta, respectively. The heavy chains' variable regions were shown in skyblue and the light chains' variable regions in limon. FAP2 binds to the Catalytic domain of PCSK9 whereas FAP2M21 binds to the CTD of PCSK9. Key residues involved in the interactions were represented as sticks models and labelled in red font for PCSK9′ key residues, black for antibody' key residues. The hydrogen bonds were shown as black dotted lines.

clinic [56,57], whereas the development of bococizumab, a humanized mAb, was terminated due to the immunogenicity and a wide individual variability in the LDL-C lowering response to bococizumab [58]. Notably, it has been shown that the LDL-C lowering efficacy of statins was significantly improved when used in combination with alirocumab or evolocumab both in randomized controlled trials and in a routine care setting [59,60]. Besides, RG7652, a fully human IgG1 mAb against PCSK9, and LY3015014, a humanized IgG4 mAb against PCSK9 are being evaluated in a randomized, double-blinded, dose-ranging, phase 2 EQUATOR trial [61], and in a randomized placebo-controlled phase 2 trial [62], respectively. Cao [63] reported that a human anti-PCSK9 antibody PA4-IgG1 was selected from a Fab phage library, which binds to PCSK9 with K_D of 1.05 nM, and dissociation rate (k_{off}, 1.66×10^{-4} s^{-1}).

In this work, we exploited a technically different scFv phage library, which was established in our lab in as early as 2014, and had been successfully utilized to isolate a fully human agonistic scFv targeting death receptor 5 [24], to discover a highly active human anti-PCSK9 antibody (Fig. 7). Firstly, we generated a potent single-chain variable fragment (scFv) named AP2M21 by screening a fully human

Table 4
Effects of FAP2M21 on serum lipids levels in hyperlipidemic mice model.

Group		Dose (mg/kg)	LDL-C (mmol/L)	TC (mmol/L)	TG (mmol/L)	HDL-C (mmol/L)
Normal group		/	0.624 ± 0.021	3.642 ± 0.161	0.921 ± 0.028	1.417 ± 0.042
Model group		/	1.560 ± 0.037$^{\#\#\#}$	5.250 ± 0.212$^{\#\#\#}$	1.351 ± 0.049$^{\#\#}$	1.340 ± 0.036
Alirocumab group	Low dose	1	1.506 ± 0.164	4.903 ± 0.071	1.320 ± 0.052	1.274 ± 0.066
	Medium dose	3	1.122 ± 0.122*	4.650 ± 0066*	1.211 ± 0.048	1.417 ± 0.088
	High dose	10	0.964 ± 0.024**	4.276 ± 0.062*	1.162 ± 0.037*	1.287 ± 0.054
FAP2M21 group	Low dose	1	1.509 ± 0.103	4.978 ± 0.153	1.333 ± 0.050	1.199 ± 0.039
	Medium dose	3	1.089 ± 0.046**	4.579 ± 0.092*	1.215 ± 0.025	1.232 ± 0.078
	High dose	10	0.979 ± 0.072**	4.373 ± 0.086*	1.182 ± 0.047*	1.348 ± 0.031

Values are expressed as means ± SEM (n = 6 per group). * $P<$ 0.05, ** $P<$ 0.01 *vs.* Model group. $^{\#\#}P<$ 0.01, $^{\#\#\#}P<$ 0.001 *vs.* Normal group (Mann-Whitney U-test).

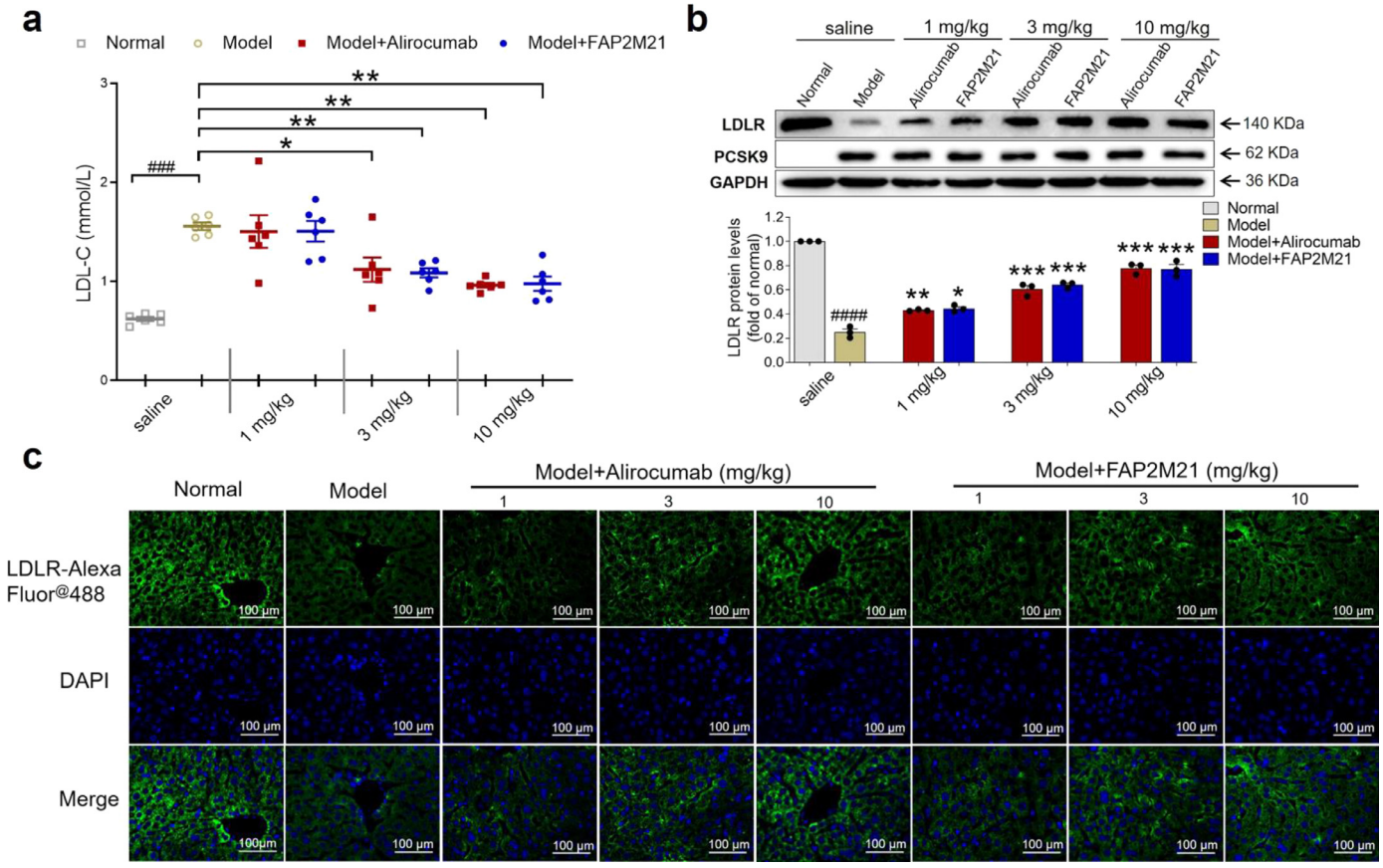

Fig. 6. *In vivo* hypolipidemic efficacy of FAP2M21 in hypercholesterolemic model mice. (a) FAP2M21 demonstrated a significant dose-dependently LDL-C lowering effect similar to alirocumab. Results were expressed as mean ± SEM (n = 6 per group). See Table 4 for detail value. (b-c) Hepatic LDLR changes in FAP2M21 or alirocumab treated C57BL/6 mice were detected by western blot (b) and Immunofluorescence (c). Meanwhile, overexpressed hPCSK9 in livers of the model mouse was also verified by using anti-hPCSK9 antibody (1:3000 dilution; Abcam). $^{*}P<$0.05, $^{**}P<$ 0.01, $^{***}P<$ 0.001 *vs.* Model group. $^{\#\#}$ $P<$ 0.01, $^{\#\#\#}$ $P<$ 0.001 *vs.* Normal group (Mann-Whitney U-test). Scale bars = 100 μm. Data are representative of 3 independent experiments with similar results.

phage display library with hPCSK9. Then, we performed two rounds of *in vitro* affinity maturation processes including CDR-targeted tailored mutagenesis and cross-cloning to further improve its affinity to PCSK9. Thereafter, considering the full-length IgG mAb being the most appropriate format for clinical applications because of its long half-life, high stability and bivalent binding property [64,65], we further constructed the full-length Fc-silenced anti-PCSK9 antibodies by fusing two anti-PCSK9 scFv variants (AP2M18 and AP2M21) to a modified human IgG1 Fc fragment with L234A/L235A/N297G mutations and C-terminal lysine deletion, thereby eliminating the immune effector functions and mitigating the potential mAb heterogeneity. Based on Bio-Layer Interferometry (BLI) analysis, it was revealed that the full-length anti-PCSK9 antibody FAP2M21 binds to hPCSK9 with a K_D as low as 1.42 nM, and a dramatically slow dissociation rate (k_{off}, 4.68 × 10^{-6} s^{-1}). Mechanically, it could be attributed to its lower binding energy (-47.51 kcal/mol) as compared to that of its parent counterpart FAP2 (-30.39 kcal/mol). Since the dissociation rate (k_{off}), also known as first-order dissociation rate constant of complex, is closely related with the lifetime of the drug-target complex [66,67], the lower dissociation rate plays a key role in prolonging the duration of antibody-antigen interaction, which has been demonstrated as a highly desirable property in therapeutic antibodies [68–70]. Due to the importance of slow k_{off}, multiple studies have been reported to use the "off-rate screening" method to isolate high-affinity antibodies [71–73].

The fully human, anti-PCSK9 antibody FAP2M21 developed in this work, binds to PCSK9 with a dramatically slow dissociation rate (k_{off}, 4.68 × 10^{-6} s^{-1}), which is approximately two orders of magnitude slower than the dissociation rate (k_{off}, 1.66 × 10^{-4} s^{-1}) of PA4-IgG1, which was generated in Cao's report [63]. Thus, the extremely slow

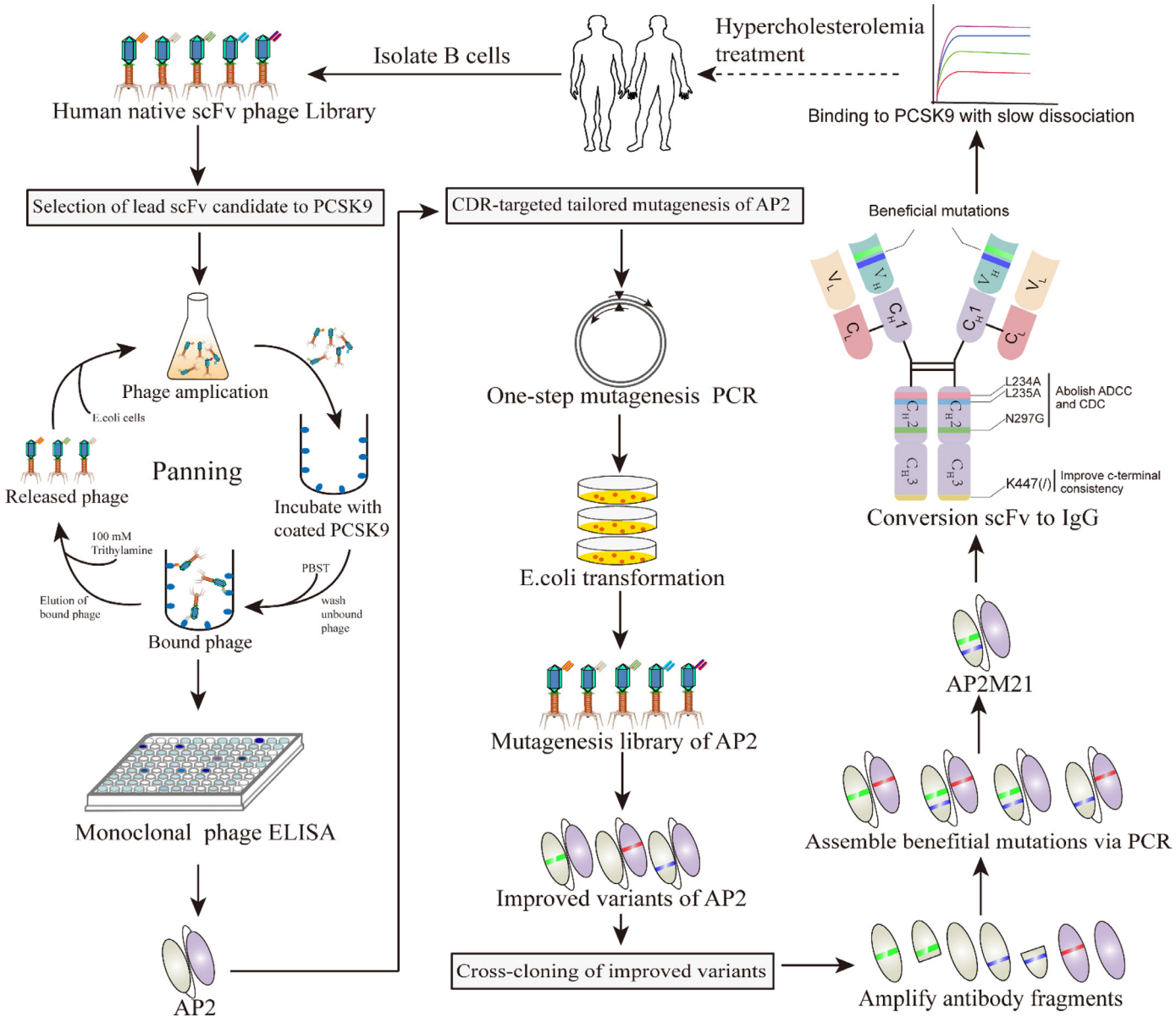

Fig. 7. Schematic pictorial representation of the development of FAP2M21. As is vividly depicted by the picture above, the optimal mutated scFv named AP2M21 was obtained from phage display biopanning and CDR-targeted tailored mutagenesis followed by a cross-cloning process. Subsequently, AP2M21 was reformatted to full-length IgG1 by fusing the effector function-silenced and C-terminal lysine deleted Fc region. FAP2M21 can bind to PCSK9 with an extremely slow dissociation rate constant and exert its hypolipidemic effect by blocking PCSK9-LDLR interaction.

dissociation rate of the full-length anti-PCSK9 antibody FAP2M21 appears to be much favourable to its druggability.

Although IgG2 Fc and IgG4 Fc fragments can be used for constructing the full-length antibody when Fc effector function is undesirable for therapeutic activity, they show decreased conformational stability relative to that of IgG1 because of their higher propensity to aggregate [74,75]. It has been observed that IgG2 Fc is not completely devoid of ADCC activity under certain conditions [76,77]. Besides, disulfide-bond reshuffling and Fab-arm exchange occurring in IgG2 and IgG4 subclasses lead to multiple heterogeneous isoforms with altered activities [78,79]. Hence, in this work we chose a modified IgG1 Fc fragment with L234A/L235A/N297G mutations, known to abolish the undesirable Fc effector functions such as ADCC and CDC activities [38,80], to construct the full-length Fc-silenced anti-PCSK9 antibodies. No information was provided in Cao's paper regarding whether the Fc was modified to construct the full-length PA4-IgG1 antibody [63].

Using molecular docking method, we showed that FAP2M21 binds the module 2 (amino acids 530–605) of the C-terminal domain (CTD) of PCSK9 (Fig. 5) which is considered to be essential for the extracellular activity of PCSK9 on cell surface LDLR [81]. Even though studies have shown that it is the catalytic domain of PCSK9 that primarily interacts with LDLR [4, 6] and antibody targeting this domain could reduce serum cholesterol in mice and nonhuman primates effectively [82], several gain- (H553R) or loss-of-function (R434W and C679X) point mutations within the CTD of PCSK9 highlight the functional significance of the C-terminal region [83–85]. Consistently, several antibodies or proteins binding to the CTD of PCSK9 such as mAb1 [86], 1G08 [87], and Annexin A2 [88], have been identified and proved able to inhibit PCSK9 function. All these PCSK9 inhibitors bind distinctive epitopes, indicating the presence of multiple epitopes within CTD of PCSK9 that can modulate circulating LDL-C levels.

The *in vivo* hypolipidemic potency of FAP2M21 was evaluated in a hyperlipidemic C57BL/6 mouse model. As expected, FAP2M21 robustly reduced the serum LDL-C and TC levels in a dose-dependent manner, with the potency comparable to the positive control alirocumab. However, both FAP2M21 and alirocumab have little effects on serum HDL-C levels. Yet, since no positive control was utilized in Cao's report [63], it is hard to know how effective the antibody PA4-IgG1 functions in lowering the serum LDL-C and TC levels *in vivo*.

In summary, we generate a novel, fully human, anti-PCSK9 IgG1 mAb FAP2M21 with a high affinity to PCSK9 and an extremely slow dissociation rate by screening a fully human scFv phage display library, *in vitro* affinity maturation as well as fusing with a modified human IgG1 Fc fragment. The data show that FAP2M21 potently inhibits PCSK9-mediated LDLR degradation and robustly lower the serum LDL-C and TC levels in a hyperlipidemic mouse model, suggesting that FAP2M21 may serve as a promising candidate for treating hypercholesterolemia and associated cardiovascular diseases.

Data sharing statement

Data supporting the findings of this study are available within the manuscript and supplementary information and are also available from the authors upon reasonable request. The heavy and light chain antibody sequences used to generate FAP2M18 and FAP2M21 are available in the GenBank database under the accession numbers: MW428281, MW428282, MW428283, and MW428284.

Contributors

M. Xu and G. Lei designed and performed research, analyzed data, and wrote the manuscript. M. Chen, K. Wang and W. Lv performed research and analyzed data. P. Zhang, T. Hu, C. Lu, Y. Mei, Z. Xu, Z. Bai, H. Hu and Y. Jiang performed research. S. Tan designed research, wrote the manuscript, and coordinated the project. S. Tan, M. Xu, G. Lei, M. Chen, K. Wang, W. Lv, P. Zhang and T. Hu verified the underlying data, and all authors gave final approval of the manuscript.

Funding

This work was funded by National Fund for Major Projects of China (2009ZX09103-653; 2013ZX09301303-006; 2018ZX09301035), The Priority Academic Program Development of Jiangsu Higher Education Institutions (PAPD), National Fund for Fostering Talents of Basic Science (NFFTBS, 3050040016), China Pharmaceutical University "Double First-Class" project (CPU2018GY15).

Declaration of Competing Interest

The authors declare no conflict of interest concerning this article.

Acknowledgements

This work was funded by National Fund for Major Projects of China (2009ZX09103-653; 2013ZX09301303-006; 2018ZX09301035), The Priority Academic Program Development of Jiangsu Higher Education Institutions (PAPD), National Fund for Fostering Talents of Basic Science (NFFTBS, 3050040016), China Pharmaceutical University "Double First-Class" project (CPU2018GY15). We would like to thank all other members of Prof. Shuhua Tan's lab for their professional support and assistance, especially Yaqiang Zhao, Yingli Zhu, Jiaqi Shen, Chenxi Zhang, and Yuting Chen for their help in manuscript proofreading and preparation.

Supplementary materials

Supplementary material associated with this article can be found in the online version at doi:10.1016/j.ebiom.2021.103250.

References

[1] Benjamin EJ, Muntner P, Alonso A, Bittencourt MS, Callaway CW, Carson AP, et al. Heart disease and stroke statistics-2019 update: a report from the American heart association. Circulation. 2019;139(10):e56–e528.
[2] Newman CB, Preiss D, Tobert JA, Jacobson TA, Page 2nd RL, Goldstein LB, et al. Statin safety and associated adverse events: a scientific statement from the American heart association. Arterioscler Thromb Vasc Biol 2019;39(2):e38–81.
[3] Seidah NG, Benjannet S, Wickham L, Marcinkiewicz J, Jasmin SB, Stifani S, et al. The secretory proprotein convertase neural apoptosis-regulated convertase 1 (NARC-1): liver regeneration and neuronal differentiation. Proc Natl Acad Sci United States Am 2003;100(3):928–33.
[4] Kwon HJ, Lagace TA, McNutt MC, Horton JD, Deisenhofer J. Molecular basis for LDL receptor recognition by PCSK9. Proc Natl Acad Sci United States Am 2008;105(6):1820–5.
[5] Wang Y, Huang Y, Hobbs HH, Cohen JC. Molecular characterization of proprotein convertase subtilisin/kexin type 9-mediated degradation of the LDLR. J Lipid Res 2012;53(9):1932–43.
[6] Lo Surdo P, Bottomley MJ, Calzetta A, Settembre EC, Cirillo A, Pandit S, et al. Mechanistic implications for LDL receptor degradation from the PCSK9/LDLR structure at neutral pH. EMBO Rep 2011;12(12):1300–5.
[7] EbioMedicine. PCSK9 inhibitors: what lies beyond monoclonal antibodies? EBioMedicine 2015;2(12):1835.
[8] Busuioc RM, Covic A, Kanbay M, Banach M, Burlacu A, Mircescu G. Protein convertase subtilisin/kexin type 9 biology in nephrotic syndrome: implications for use as therapy. Nephrol Dial Transplant 2020;35(10):1663–74.
[9] Angouridis A, Georgoula M, Tellis CC, Filippatos TD, Tselepis A, Liberopoulos E, et al. Serum PCSK9 levels are increased in obese subjects and negatively correlated with a mediterranean diet score. Atherosclerosis 2018;275:e251–e2.
[10] Sahebkar A, Simental-Mendia LE, Guerrero-Romero F, Golledge J, Watts GF. Effect of statin therapy on plasma proprotein convertase subtilisin kexin 9 (PCSK9) concentrations: a systematic review and meta-analysis of clinical trials. Diabetes Obes Metab 2015;17(11):1042–55.
[11] Lu RM, Hwang YC, Liu IJ, Lee CC, Tsai HZ, Li HJ, et al. Development of therapeutic antibodies for the treatment of diseases. J Biomed Sci 2020;27(1):1.
[12] Barderas R, Benito-Pena E. The 2018 nobel prize in chemistry: phage display of peptides and antibodies. Anal Bioanal Chem 2019;411(12):2475–9.
[13] Zhao A, Tohidkia MR, Siegel DL, Coukos G, Omidi Y. Phage antibody display libraries: a powerful antibody discovery platform for immunotherapy. Crit Rev Biotechnol 2016;36(2):276–89.
[14] Ho M, Pastan I. In Vitro antibody affinity maturation targeting germline hotspots editor. In: Dimitrov AS, editor. Therapeutic antibodies: methods and protocols. Totowa, NJ: Humana Press; 2009. p. 293–308.
[15] Bain B, Brazil M. Adalimumab. Nat Rev Drug Discovery. 2003;2(9):693-4.
[16] Frenzel A, Schirrmann T, Hust M. Phage display-derived human antibodies in clinical development and therapy. mAbs 2016;8(7):1177–94.
[17] Nixon AE, Sexton DJ, Ladner RC. Drugs derived from phage display: from candidate identification to clinical practice. mAbs 2014;6(1):73–85.
[18] Gonzalez-Munoz A, Bokma E, O'Shea D, Minton K, Strain M, Vousden K, et al. Tailored amino acid diversity for the evolution of antibody affinity. mAbs 2012;4(6):664–72.
[19] Tiller KE, Chowdhury R, Li T, Ludwig SD, Sen S, Maranas CD, et al. Facile affinity maturation of antibody variable domains using natural diversity mutagenesis. Front Immunol 2017;8:986.
[20] Muller BH, Savatier A, L'Hostis G, Costa N, Bossus M, Michel S, et al. In vitro affinity maturation of an anti-PSA antibody for prostate cancer diagnostic assay. J Mol Biol 2011;414(4):545–62.
[21] Steidl S, Ratsch O, Brocks B, Durr M, Thomassen-Wolf E. In vitro affinity maturation of human GM-CSF antibodies by targeted CDR-diversification. Mole Immunol 2008;46(1):135–44.
[22] Hernández G, Osnaya VG, Pérez-Martínez X. Conservation and variability of the AUG initiation codon context in eukaryotes. Trends Biochem Sci 2019;44(12):1009–21.
[23] Stuible M, Burlacu A, Perret S, Brochu D, Paul-Roc B, Baardsnes J, et al. Optimization of a high-cell-density polyethylenimine transfection method for rapid protein production in CHO-EBNA1 cells. J Biotechnol 2018;281:39–47.
[24] Lei G, Xu M, Xu Z, Gu L, Lu C, Bai Z, et al. A novel fully human agonistic single chain fragment variable antibody targeting death receptor 5 with potent antitumor activity in vitro and in vivo. Int J Mole Sci 2017;18(10):2064.
[25] Kang AS, Barbas CF, Janda KD, Benkovic SJ, Lerner RA. Linkage of recognition and replication functions by assembling combinatorial antibody Fab libraries along phage surfaces. Proc Natl Acad Sci United States Am 1991;88(10):4363–6.
[26] Whitelegg NR, Rees AR. WAM: an improved algorithm for modelling antibodies on the WEB. Protein Eng 2000;13(12):819–24.
[27] Whitelegg N, Rees AR. Antibody variable regions: toward a unified modeling method. Methods Mole Biol 2004;248:51–91.
[28] Swindells MB, Porter CT, Couch M, Hurst J, Abhinandan KR, Nielsen JH, et al. abYsis: Integrated antibody sequence and structure-management, analysis, and prediction. J Mole Biol 2017;429(3):356–64.
[29] Xu M, Hu S, Ding B, Fei C, Wan W, Hu D, et al. Design and construction of small perturbation mutagenesis libraries for antibody affinity maturation using massive microchip-synthesized oligonucleotides. J Biotechnol 2015;194:27–36.
[30] Hu D, Hu S, Wan W, Xu M, Du R, Zhao W, et al. Effective optimization of antibody affinity by phage display integrated with high-throughput DNA synthesis and sequencing technologies. PLoS One 2015;10(6):e0129125.

[31] Zheng L. An efficient one-step site-directed and site-saturation mutagenesis protocol. Nucleic Acids Res 2004;32(14):e115.
[32] Gu L, Ye P, Li H, Wang Y, Xu Y, Tian Q, et al. Lunasin attenuates oxidant-induced endothelial injury and inhibits atherosclerotic plaque progression in ApoE(-/-) mice by up-regulating heme oxygenase-1 via PI3K/Akt/Nrf2/ARE pathway. FASEB J 2019;33(4):4836–50.
[33] Ly K, Saavedra YG, Canuel M, Routhier S, Desjardins R, Hamelin J, et al. Annexin A2 reduces PCSK9 protein levels via a translational mechanism and interacts with the M1 and M2 domains of PCSK9. J Biol Chem 2014;289(25):17732–46.
[34] Lu Y, Xiao S, Yuan M, Gao Y, Sun J, Xue C. Using overlap-extension PCR technique to fusing genes for constructing recombinant plasmids. J Basic Microbiol 2018;58 (3):273–6.
[35] Wines BD, Powell MS, Parren PW, Barnes N, Hogarth PM. The IgG Fc contains distinct Fc receptor (FcR) binding sites: the leukocyte receptors Fc gamma RI and Fc gamma RIIa bind to a region in the Fc distinct from that recognized by neonatal FcR and protein A. J Immunol 2000;164(10):5313–8.
[36] Hessell AJ, Hangartner L, Hunter M, Havenith CE, Beurskens FJ, Bakker JM, et al. Fc receptor but not complement binding is important in antibody protection against HIV. Nature 2007;449(7158):101–4.
[37] Jefferis R. Recombinant antibody therapeutics: the impact of glycosylation on mechanisms of action. Trends Pharmacol Sci 2009;30(7):356–62.
[38] Jacobsen FW, Stevenson R, Li C, Salimi-Moosavi H, Liu L, Wen J, et al. Engineering an IgG scaffold lacking effector function with optimized developability. J Biol Chem 2017;292(5):1865–75.
[39] Liu H, Gaza-Bulseco G, Faldu D, Chumsae C, Sun J. Heterogeneity of monoclonal antibodies. J Pharm Sci 2008;97(7):2426–47.
[40] Dick Jr. LW, Qiu D, Mahon D, Adamo M, Cheng KC. C-terminal lysine variants in fully human monoclonal antibodies: investigation of test methods and possible causes. Biotechnol Bioeng 2008;100(6):1132–43.
[41] Xu Y, Gao J, Gong Y, Chen M, Chen J, Zhao W, et al. Hsa-miR-140-5p down-regulates LDL receptor and attenuates LDL-C uptake in human hepatocytes. Atherosclerosis 2020;297:111–9.
[42] Dunbar J, Krawczyk K, Leem J, Marks C, Nowak J, Regep C, et al. SAbPred: a structure-based antibody prediction server. Nucleic Acids Res 2016;44(W1):W474–W8.
[43] Yan Y, Tao H, He J, Huang SY. The HDOCK server for integrated protein-protein docking. Nat Protoc 2020;15(5):1829–52.
[44] Weng G, Wang E, Wang Z, Liu H, Zhu F, Li D, et al. HawkDock: a web server to predict and analyze the protein-protein complex based on computational docking and MM/GBSA. Nucleic Acids Res 2019;47(W1):W322–W30.
[45] Miao CH, Thompson AR, Loeb K, Ye X. Long-term and therapeutic-level hepatic gene expression of human factor IX after naked plasmid transfer in vivo. Mol Ther 2001;3(6):947–57.
[46] Suda T, Liu D. Hydrodynamic gene delivery: its principles and applications. Mol Ther 2007;15(12):2063–9.
[47] Tietge UJ. Hyperlipidemia and cardiovascular disease: inflammation, dyslipidemia, and atherosclerosis. Curr Opin Lipidol 2014;25(1):94–5.
[48] Rader DJ, Daugherty A. Translating molecular discoveries into new therapies for atherosclerosis. Nature 2008;451(7181):904–13.
[49] Stone NJ, Robinson JG, Lichtenstein AH, Bairey Merz CN, Blum CB, Eckel RH, et al. 2013 ACC/AHA guideline on the treatment of blood cholesterol to reduce atherosclerotic cardiovascular risk in adults: a report of the American college of cardiology/American heart association task force on practice guidelines. Circulation 2014;129(25 Suppl 2):S1–45.
[50] Grundy SM. An international atherosclerosis society position paper: global recommendations for the management of dyslipidemia. J Clin Lipidol 2013;7 (6):561–5.
[51] Brown MS, Goldstein JL. A receptor-mediated pathway for cholesterol homeostasis (nobel lecture). Science 1986;232(4746):34–47.
[52] Endo A, Tsujita Y, Kuroda M, Tanzawa K. Inhibition of cholesterol synthesis in vitro and in vivo by ML-236A and ML-236B, competitive inhibitors of 3-Hydroxy-3-methylglutaryl-coenzyme a reductase. Eur J Biochem 1977;77(1):31–6.
[53] Rudling M, Angelin B, Stahle L, Reihner E, Sahlin S, Olivecrona H, et al. Regulation of hepatic low-density lipoprotein receptor, 3-hydroxy-3-methylglutaryl coenzyme A reductase, and cholesterol 7alpha-hydroxylase mRNAs in human liver. J Clin Endocrinol Metab 2002;87(9):4307–13.
[54] Dong B, Wu M, Li H, Kraemer FB, Adeli K, Seidah NG, et al. Strong induction of PCSK9 gene expression through HNF1alpha and SREBP2: mechanism for the resistance to LDL-cholesterol lowering effect of statins in dyslipidemic hamsters. J Lipid Res 2010;51(6):1486–95.
[55] Dong B, Singh AB, Shende VR, Liu J. Hepatic HNF1 transcription factors control the induction of PCSK9 mediated by rosuvastatin in normolipidemic hamsters. Int J Mol Med 2017;39(3):749–56.
[56] Robinson JG, Farnier M, Krempf M, Bergeron J, Luc G, Averna M, et al. Efficacy and safety of alirocumab in reducing lipids and cardiovascular events. N Engl J Med 2015;372(16):1489–99.
[57] Sabatine MS, Giugliano RP, Keech AC, Honarpour N, Wiviott SD, Murphy SA, et al. Evolocumab and Clinical Outcomes in Patients with Cardiovascular Disease. N Engl J Med 2017;376(18):1713–22.
[58] Ridker PM, Tardif JC, Amarenco P, Duggan W, Glynn RJ, Jukema JW, et al. Lipid-reduction variability and antidrug-antibody formation with bococizumab. N Engl J Med 2017;376(16):1517–26.
[59] Reiner Ž. PCSK9 inhibitors in clinical practice: Expectations and reality. Atherosclerosis 2018;270:187–8.
[60] Stoekenbroek RM, Hartgers ML, Rutte R, de Wijer DD, Stroes ESG, Hovingh GK. PCSK9 inhibitors in clinical practice: delivering on the promise? Atherosclerosis 2018;270:205–10.
[61] Baruch A, Mosesova S, Davis JD, Budha N, Vilimovskij A, Kahn R, et al. Effects of RG7652, a monoclonal antibody against PCSK9, on LDL-C, LDL-C subfractions, and inflammatory biomarkers in patients at high risk of or with established coronary heart disease (from the phase 2 EQUATOR study). Am J Cardiol 2017;119 (10):1576–83.
[62] Kastelein JJ, Nissen SE, Rader DJ, Hovingh GK, Wang MD, Shen T, et al. Safety and efficacy of LY3015014, a monoclonal antibody to proprotein convertase subtilisin/kexin type 9 (PCSK9): a randomized, placebo-controlled Phase 2 study. Eur Heart J 2016;37(17):1360–9.
[63] Cao Y, Yang H, Zhou X, Mao H, Gao T, Hu Z, et al. Selection and characterization of human PCSK9 antibody from phage displayed antibody library. Biochem Biophys Res Commun 2015;463(4):712–8.
[64] Yang C, Gao X, Gong R. Engineering of Fc fragments with optimized physicochemical properties implying improvement of clinical potentials for fc-based therapeutics. Front Immunol 2017;8:1860.
[65] Walsh G. Biopharmaceutical benchmarks 2018. Nat Biotechnol 2018;36 (12):1136–45.
[66] Vauquelin G, Charlton SJ. Long-lasting target binding and rebinding as mechanisms to prolong in vivo drug action. Br J Pharmacol 2010;161(3):488–508.
[67] Copeland RA. The dynamics of drug-target interactions: drug-target residence time and its impact on efficacy and safety. Expert Opin Drug Discovery 2010;5 (4):305–10.
[68] Bottermann M, Lode HE, Watkinson RE, Foss S, Sandlie I, Andersen JT, et al. Antibody-antigen kinetics constrain intracellular humoral immunity. Sci Reports. 2016;6:37457.
[69] Lee S, Greenlee EB, Amick JR, Ligon GF, Lillquist JS, Natoli Jr. EJ, et al. Inhibition of ErbB3 by a monoclonal antibody that locks the extracellular domain in an inactive configuration. PNAS 2015;112(43):13225–30.
[70] XU H, Hu J, Cheung NV. Induction of tumor cell death by anti-GD2 monoclonal antibodies (MoAb): Requirement of antibody Fc and a long residence time (slow koff). J Clin Oncol 2007;25(18_suppl):13507.
[71] Ylera F, Harth S, Waldherr D, Frisch C, Knappik A. Off-rate screening for selection of high-affinity anti-drug antibodies. Anal Biochem 2013;441(2):208–13.
[72] Pirez-Schirmer M, Rossotti M, Badagian N, Leizagoyen C, Brena BM, Gonzalez-Sapienza G. Comparison of three antihapten VHH selection strategies for the development of highly sensitive immunoassays for microcystins. Anal Chem 2017;89(12):6800–6.
[73] Liu L. Efficient hit and lead compound evaluation strategy based on off-rate screening by surface plasmon resonance. J Med Chem 2014;57(7):2843–4.
[74] Skamris T, Tian X, Thorolfsson M, Karkov HS, Rasmussen HB, Langkilde AE, et al. Monoclonal antibodies follow distinct aggregation pathways during production-relevant acidic incubation and neutralization. Pharm Res 2016;33(3):716–28.
[75] Farys M, Gibson D, Lewis AP, Lewis W, Kucia-Tran R. Isotype dependent on-column non-reversible aggregation of monoclonal antibodies. Biotechnol Bioeng 2018;115(5):1279–87.
[76] Schneider-Merck T, Lammerts van Bueren JJ, Berger S, Rossen K, van Berkel PH, Derer S, et al. Human IgG2 antibodies against epidermal growth factor receptor effectively trigger antibody-dependent cellular cytotoxicity but, in contrast to IgG1, only by cells of myeloid lineage. J Immunol 2010;184(1):512–20.
[77] Koch T, Derer S, Staudinger M, Rossen K, Glorius P, Peipp M, et al. Antibody-dependent cellular cytotoxicity in patients on chronic hemodialysis. Am J Nephrol 2013;38(5):379–87.
[78] van der Neut Kolfschoten M, Schuurman J, Losen M, Bleeker WK, Martinez-Martinez P, Vermeulen E, et al. Anti-inflammatory activity of human IgG4 antibodies by dynamic Fab arm exchange. Science 2007;317(5844):1554–7.
[79] Dillon TM, Ricci MS, Vezina C, Flynn GC, Liu YD, Rehder DS, et al. Structural and functional characterization of disulfide isoforms of the human IgG2 subclass. J Biol Chem 2008;283(23):16206–15.
[80] Strohl WR. Optimization of Fc-mediated effector functions of monoclonal antibodies. Curr Opin Biotechnol 2009;20(6):685–91.
[81] Saavedra YG, Day R, Seidah NG. The M2 module of the Cys-His-rich domain (CHRD) of PCSK9 protein is needed for the extracellular low-density lipoprotein receptor (LDLR) degradation pathway. J Biol Chem 2012;287(52):43492–501.
[82] Chan JCY, Piper DE, Cao Q, Liu D, King C, Wang W, et al. A proprotein convertase subtilisin/kexin type 9 neutralizing antibody reduces serum cholesterol in mice and nonhuman primates. PNAS 2009;106(24):9820–5.
[83] Kotowski IK, Pertsemlidis A, Luke A, Cooper RS, Vega GL, Cohen JC, et al. A spectrum of PCSK9 alleles contributes to plasma levels of low-density lipoprotein cholesterol. Am J Hum Genet 2006;78(3):410–22.
[84] Hooper AJ, Marais AD, Tanyanyiwa DM, Burnett JR. The C679X mutation in PCSK9 is present and lowers blood cholesterol in a Southern African population. Atherosclerosis 2007;193(2):445–8.
[85] Dubuc G, Tremblay M, Pare G, Jacques H, Hamelin J, Benjannet S, et al. A new method for measurement of total plasma PCSK9: clinical applications. J Lipid Res 2010;51(1):140–9.
[86] Schiele F, Park J, Redemann N, Luippold G, Nar H. An antibody against the C-terminal domain of PCSK9 lowers LDL cholesterol levels in vivo. J Mol Biol 2014;426 (4):843–52.
[87] Ni YG, Condra JH, Orsatti L, Shen X, Di Marco S, Pandit S, et al. A proprotein convertase subtilisin-like/kexin type 9 (PCSK9) C-terminal domain antibody antigen-binding fragment inhibits PCSK9 internalization and restores low density lipoprotein uptake. J Biol Chem 2010;285(17):12882–91.
[88] Mayer G, Poirier S, Seidah NG. Annexin A2 is a C-terminal PCSK9-binding protein that regulates endogenous low density lipoprotein receptor levels. J Biol Chem 2008;283(46):31791–801.